Article

Cell

# Restoring the Sense of Touch Using a Sensorimotor Demultiplexing Neural Interface

## Graphical Abstract

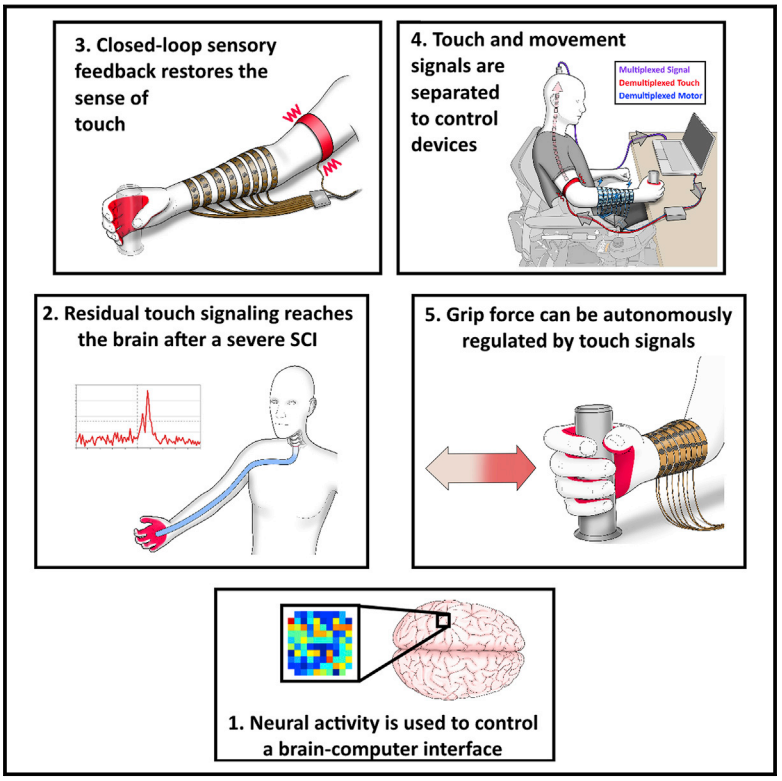


## Highlights

- Following spinal cord injury, subperceptual touch signals affect the human motor cortex
- A brain-computer interface uses subperceptual signals to restore the sense of touch
- Sensorimotor function is further enhanced using demultiplexed sensorimotor signals
- Touch-regulated grip force can automate movement cascades and grip reanimation

## Authors

Patrick D. Ganzer, Samuel C. Colachis 4th, Michael A. Schwemmer, ..., Doug J. Weber, Marcia A. Bockbrader, Gaurav Sharma

## Correspondence

ganzer@battelle.org

## In Brief

Sensation is restored to the hand of a participant with quadriplegia by a brain-computer interface that transforms residual, subperceptual touch signals into conscious perception.

Ganzer et al., 2020, Cell *181*, 1–11
May 14, 2020 © 2020 Elsevier Inc.
https://doi.org/10.1016/j.cell.2020.03.054

CellPress

Please cite this article in press as: Ganzer et al., Restoring the Sense of Touch Using a Sensorimotor Demultiplexing Neural Interface, Cell (2020), https://doi.org/10.1016/j.cell.2020.03.054

Article

Cell

# Restoring the Sense of Touch Using a Sensorimotor Demultiplexing Neural Interface

Patrick D. Ganzer,[1,5,*] Samuel C. Colachis 4th,[1] Michael A. Schwemmer,[3] David A. Friedenberg,[3] Collin F. Dunlap,[1,2] Carly E. Swiftney,[1] Adam F. Jacobowitz,[1] Doug J. Weber,[1,4] Marcia A. Bockbrader,[2] and Gaurav Sharma[1]

[1]Medical Devices and Neuromodulation, Battelle Memorial Institute, 505 King Avenue, Columbus, OH 43201, USA
[2]Department of Physical Medicine and Rehabilitation, The Ohio State University, Columbus, OH 43210, USA
[3]Advanced Analytics and Health Research, Battelle Memorial Institute, 505 King Avenue, Columbus, OH 43201, USA
[4]Department of Bioengineering, University of Pittsburgh, 4200 Fifth Avenue, Pittsburgh, PA 15260, USA
[5]Lead Contact
*Correspondence: ganzer@battelle.org
https://doi.org/10.1016/j.cell.2020.03.054

## SUMMARY

**Paralyzed muscles can be reanimated following spinal cord injury (SCI) using a brain-computer interface (BCI) to enhance motor function alone. Importantly, the sense of touch is a key component of motor function. Here, we demonstrate that a human participant with a clinically complete SCI can use a BCI to simultaneously reanimate both motor function and the sense of touch, leveraging residual touch signaling from his own hand. In the primary motor cortex (M1), residual subperceptual hand touch signals are simultaneously demultiplexed from ongoing efferent motor intention, enabling intracortically controlled closed-loop sensory feedback. Using the closed-loop demultiplexing BCI almost fully restored the ability to detect object touch and significantly improved several sensorimotor functions. Afferent grip-intensity levels are also decoded from M1, enabling grip reanimation regulated by touch signaling. These results demonstrate that subperceptual neural signals can be decoded from the cortex and transformed into conscious perception, significantly augmenting function.**

## INTRODUCTION

Spinal cord injury (SCI) damages sensorimotor circuits leading to paralysis, an impaired sense of agency, and sensory dysfunction. Interestingly, recent evidence suggests that a severe clinically complete SCI does not entirely block ascending sensory information transmission from skin innervated below the lesion (Wrigley et al., 2018; Awad et al., 2015; Ioannides et al., 2002; Sabbah et al., 2002). These important studies demonstrate that, even years after SCI, tactile stimuli that the patients cannot feel evoke changes in cortical activity. "Discomplete" SCIs are now being investigated—where no clinical evidence of fiber tract function is detectable, but spared fibers may affect some physiological activity (Dimitrijevic, 1987; Sherwood et al., 1992; Finnerup et al., 2004; Wrigley et al., 2018; Awad et al., 2015; Ioannides et al., 2002; Sabbah et al., 2002). It is estimated that "sensory discomplete" SCI occurs in a considerable proportion of patients with a clinically complete SCI (~50 %; Wrigley et al., 2018; Finnerup et al., 2004). These clinical studies represent a set of critical findings. The existence of spared somatosensory fibers, and therefore residual somatosensory information, can potentially be leveraged for functional benefit in patients living with a severe SCI.

In this study, we assessed the hypothesis that a brain-computer interface (BCI) could leverage sensory discompleteness, enhance subperceptual touch events, and simultaneously restore both the sense of touch and motor function in a participant with a clinically complete SCI. The study's participant is chronically paralyzed from a clinically complete AIS-A C5 SCI (American Spinal Injury Association Impairment Scale, grade A) and has an intracortical recording array implanted in the primary motor cortex (M1) for BCI recordings. During BCI operation, the participant uses his own hand, addressing a major need of patients with SCI (Anderson, 2004; Snoek et al., 2004; Blabe et al., 2015).

Several BCI studies have targeted the motor cortex to decode motor intention alone (Lebedev and Nicolelis, 2017; Hochberg et al., 2012; Collinger et al., 2013; Gilja et al., 2015; Simeral et al., 2011; Jarosiewicz et al., 2015; Bockbrader et al., 2018; Moxon and Foffani, 2015; Bouton et al., 2016; Friedenberg et al., 2017; Sharma et al., 2016; Skomrock et al., 2018; Schwemmer et al., 2018; Colachis et al., 2018; Ajiboye et al., 2017; Bockbrader et al., 2019). Motor intention decoded from M1 is then used to enhance motor control via a robotic limb, assistive device, or the participant's own hand via functional electrical stimulation (FES). Sensory discompleteness may allow for touch-related sensory information transmission to the BCI recording site in M1.

If so, this residual touch-related sensory information could be used for restoring the sense of touch. Sensory function can potentially be augmented using a BCI that can decipher residual sensory neural activity from the impaired hand and dynamically translate this into closed-loop sensory feedback that the user can perceive. The sense of touch is critical for multiple aspects of motor control (Johansson and Flanagan, 2009). Beyond restoring the sense of touch alone, a BCI can potentially restore both sensory and motor function simultaneously in patients with SCI, even while the participants use their own hands (Anderson, 2004; Snoek et al., 2004; Blabe et al., 2015).

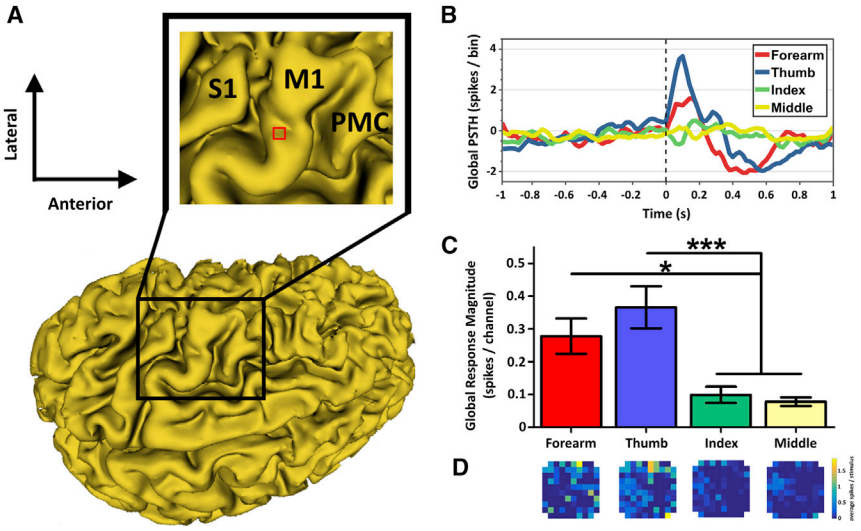


**Figure 1. Skin Stimulation on the Arm and Hand Evokes Robust Neural Responses in the Contralateral Primary Motor Cortex (M1) following Cervical Spinal Cord Injury**

(A) Pseudocolored 3D reconstruction of the participant's cerebrum using T1 magnetic resonance imaging. Red box depicts the microelectrode recording array implanted in left M1 (S1, primary somatosensory cortex; PMC, premotor cortex).

(B) A peri-stimulus time histogram (PSTH) was used to quantify neural modulation in M1 (skin stimulation occurs at time 0, vertical dashed line). Stimulation of the forearm or thumb evoked time locked multiunit activation, with smaller neural responses from index or middle.

(C) Stimulation of the forearm and thumb evoked significantly larger global response magnitudes compared to index or middle (*$p < 0.05$; ***$p < 0.001$).

(D) Color-coded representations of multiunit response magnitudes across the microelectrode recording array are shown below the labels in (C) for each stimulation location (color scaling: blues = no or small neural responses, yellow = large neural responses; units: average spikes/stimulus).

These results support the hypothesis that somatosensory stimuli evoke robust neural modulation in contralateral M1 following cervical SCI (data in B–D is for the maximum stimulation intensity; see Figure S2 for corresponding data at the minimum stimulation intensity). See Evoked Peri-Stimulus Time Histograms in the STAR Methods for additional data-processing details. Data presented are mean ± SEM.

See also Figures S1, S2, and S3.

Unfortunately, no studies to date have reported touch-related electrophysiological activity in human M1 following severe AIS-A SCI (Wrigley et al., 2018; Awad et al., 2015; Ioannides et al., 2002; Sabbah et al., 2002). Even in uninjured humans, there is significant evidence of a separation between touch and movement representations in the cortex (Harding-Forrester and Feldman, 2018; Kaas, 2012; Goldring and Ratcheson, 1972; Roux et al., 2018; Ibáñez et al., 1995; Stippich et al., 1999; Kurth et al., 1998). Furthermore, decoding sensory and motor information simultaneously for closed-loop BCI purposes is challenging. Sensory and motor neural signals may be multiplexed (Akam and Kullmann, 2014) together at the BCI recording site, significantly complicating the simultaneous and reliable decoding of multiple device control signals.

Exciting technology now exists to restore sensorimotor function using a BCI-controlled robotic limb (Flesher et al., 2019). However, no technologies exist for restoring both motor function and the sense of touch, using the participant's own hand (Anderson, 2004; Snoek et al., 2004; Blabe et al., 2015). Using the participant's hand is significantly challenging, as touch transducing systems are dramatically impacted centrally by the spinal lesion following a clinically complete SCI. This can potentially block ascending touch signaling. Furthermore, residual touch-related sensory signaling from the hand may be disrupted during challenging active states and limb reanimation.

## RESULTS

### Severe Clinically Complete SCI Leads to Significant Deficits in Hand Sensory Function

In our initial set of experiments, we sought to perform sensorimotor signal demultiplexing from M1, to enable a BCI system capable of simultaneously controlling multiple devices for enhancing both motor and sensory hand function. In principle, this potential BCI technology would leverage sensory discompleteness using residual touch-related signaling from the hand. All experiments were performed in a chronically paralyzed participant with an AIS-A C5 SCI. We first assessed the participant's residual hand sensory function (in the absence of visual feedback; Kirshblum et al., 2011). He was unable to perceive mechanical sensory stimuli to skin innervated below spinal level C6 (clinical tactile assay: Figure S1A). This sensory impairment was also present during FES-mediated object grip. For example, the participant either operated at chance levels or was completely unable to report whether he was gripping an object in the absence of visual feedback (Figure S1B), a significant sensory impairment further contributing to motor dysfunction.

### Residual Sensory Information from Insensate Hand Dermatomes Modulates M1 Neural Activity

We next investigated whether residual sensory information could significantly modulate neural activity following skin stimulation (Figures S1C–S1F). Sensory stimuli robustly modulated contralateral M1 (Figure 1; Figure S2). Stimulation of skin innervated from above or at the C5 SCI evoked time-locked neural modulation, lasting ~10 times longer than the stimulus duration (Figure 1B). Stimuli applied to skin innervated from below the SCI (index and middle) evoked modest neural modulation in M1, with stimulation to the forearm and thumb evoking significantly larger responses (Figure 1C: $F[3,380] = 9.8$, $p < 0.001$, Figure 1D). As expected, separate control experiments demonstrated little to no M1 activation following sensory stimuli to the left arm, ipsilateral to the recording array (Figure S3). These results support the hypothesis that sensory stimuli to skin innervated from both above and below the clinically complete SCI significantly modulates M1.

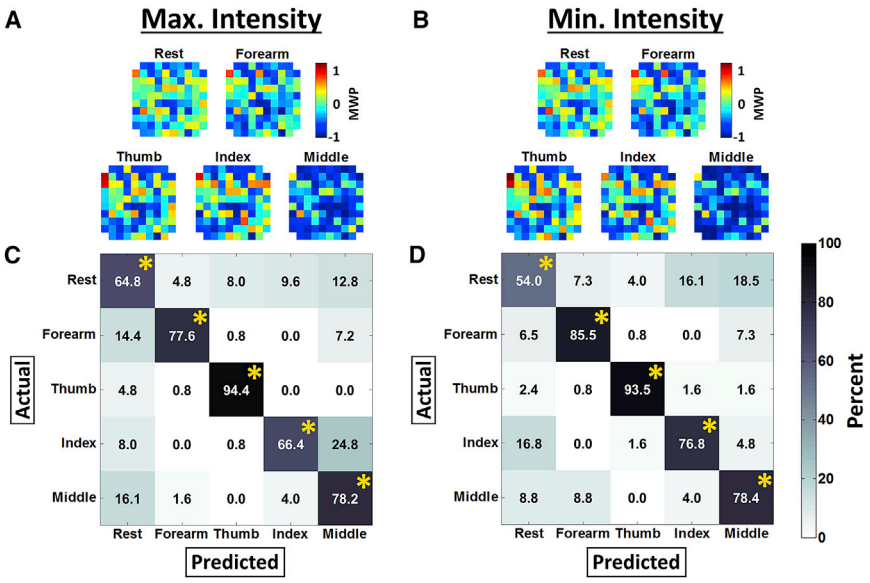


**Figure 2. Evoked Sensory Activity in M1 is Decodable Across Skin Locations**

(A and B) Color-coded representations of average mean wavelet power (MWP) across the microelectrode recording array are shown for each skin stimulation location (forearm, thumb, index, or middle) or a rest period for the maximum (A) or minimum intensities (B) (MWP maps are averaged across all recordings). Support vector machine (SVM) decoders were built using MWP recorded during stimulation at a given skin location or for a rest period (see Decoding Passive Sensory Stimulation in the STAR Methods).

(C and D) These passive sensory decoders reliably classified sensory stimulus location, demonstrating significant sensitivity above chance with low false-positive rates for both the maximum (C) and minimum stimulation intensities (D) (confusion matrices show color-coded decoder response values, units = percentage; *significantly above chance at $p < 0.001$). These results support the hypothesis that sensory activity can be demultiplexed from neural activity in M1.

## Sensory Activity in M1 Can Be Reliably Decoded during Passive Stimulation or Active Object Touch

Next, we explored whether this sensory activity can be decoded from M1. Decodable sensory events could control a feedback device for improving the impaired sense of touch. We trained a support vector machine (SVM) to detect the skin region being passively stimulated (i.e., a "passive sensory decoder"), given the underlying neural activity. Sensory stimulus location was reliably decoded from M1 across a period of several months, performing significantly above chance with low false-positive rates (Figure 2). Interestingly, passive sensory decoders for locations that the participant can feel (forearm and thumb) performed equivalently to passive sensory decoders for locations that the participant largely cannot feel (index and middle) (Figure 3). This result demonstrates the ability to decode residual sensory neural activity from M1 that is below conscious perception, from functionally relevant hand dermatomes. Furthermore, this intracortical electrophysiological evidence of sensory discompleteness extends previous studies using noninvasive imaging of evoked activity (Wrigley et al., 2018; Awad et al., 2015; Ioannides et al., 2002; Sabbah et al., 2002).

Residual sensory activity could also be decoded in a more challenging context during active object touch using a separate SVM (i.e., a "touch decoder"; Figure 4; see STAR Methods). During validation experiments, touch-decoder activation was synchronized to force application from the hand (Figure S4) and performed with high responsiveness during object touch events (~84%; Figure 4A, "touch"; $F[4,85] = 777$, $p < 0.001$; Video S1, A). As expected, the touch decoder was not activated during control cues lacking touch events (Figure 4A, No Touch; Video S1, panels B and C; "rest" occurs when the cued period is off). Specifically, a subset of control cues assessed hand proprioception events. Scripted FES that opened or closed the hand, without object touch, did not significantly activate the touch decoder (touch-decoder responsiveness: hand open = 3.7%, hand closed = 6.2%), demonstrating that hand-muscle proprioceptive signaling does not significantly contribute to touch decoding. These results reveal that residual sensory neural activity can be decoded reliably from M1 during active object manipulation.

## Real-Time Closed-Loop Sensory Feedback Controlled by Touch Decoders Restores Object Touch Detection

The participant was next interfaced with a vibrotactile array on the right bicep, to enable closed-loop sensory feedback (Figure 4B). This interface was controlled in real time by a touch decoder, to enhance the perception of hand sensory events that are significantly impaired following SCI. The closed-loop sensory feedback system was able to detect residual touch-related sensory signals from up to the C8 spinal level, therefore including the insensate regions of the hand (using clinical tactile assay of hand dermatomes; see STAR Methods). Without using the closed-loop feedback system, the participant operated at chance levels when asked to report whether he was gripping an object (Figure 4C, white; in the absence of visual feedback, Kirshblum et al., 2011), largely due to being completely insensate on the vast majority of his hand (clinical tactile assay: Figure S1A). Closed-loop sensory feedback enabled improved object touch detection from chance levels to an over 90% detection rate (Figure 4C, gray; $t(30) = 3.5$, $p = 0.001$; Figure 4D) compared to control (Figure 4C, white). Therefore, subperceptual grip detection at chance levels was significantly enhanced using closed-loop sensory feedback. These significant sensory improvements were enabled by subperceptual sensory neural activity during grip events that is demultiplexed from M1 and enhanced into conscious perception.

## Sensory and Motor Events in M1 Can Be Simultaneously Decoded to Enable "Sensorimotor Demultiplexing" BCI Control and Enhancement of Sensorimotor Function

We next assessed the hypothesis that afferent and efferent activity in M1 can be demultiplexed to simultaneously control devices

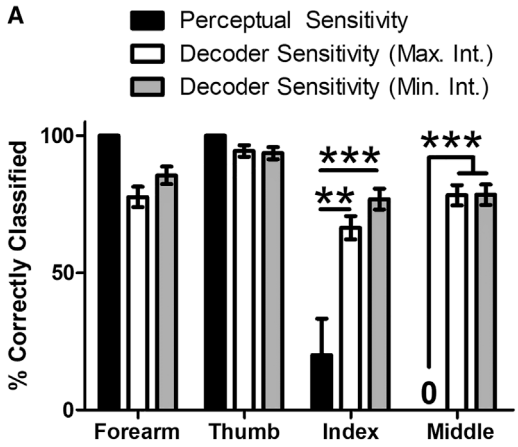


**Figure 3. Passive Sensory Decoders Accurately Decipher Subperceptual Neural Activity**

(A) We also assessed the participant's perceptual sensitivity (related to the data reported in Figure 2). We defined perceptual sensitivity as the ability of the participant to decipher whether stimulation was simply felt during a given train of stimuli (at the minimum or maximum intensity). As expected, the participant was able to feel stimuli to skin innervated from above or at the level of the SCI at a high rate (forearm and thumb) and was essentially unable to feel stimuli to skin innervated from below the level of the SCI (index and middle). Interestingly, passive sensory decoder sensitivities were significantly higher compared to the participant's perceptual sensitivity for stimuli he largely cannot feel (index, $F[2,257] = 8.1$, $p < 0.001$; middle, $F[2,256] = 17.8$, $p < 0.001$; $^{**}p < 0.01$, $^{***}p < 0.001$; decoder sensitivity values repeated from Figure 2). These results demonstrate the ability to decode residual sensory neural activity that is largely below conscious perception. Data presented are mean ± SEM.

for sensory feedback and FES, constituting a "sensorimotor demultiplexing" BCI. The sensorimotor demultiplexing BCI system is shown in Figure 5A. The touch decoder is used to control closed-loop vibrotactile sensory feedback (red band on bicep) and enhance hand-touch events. The motor decoder is used to simultaneously control FES of the arm (blue bands on forearm) and produce the desired hand movement. Real-time sensorimotor demultiplexing was demonstrated during a modified grasp and release test (GRT; Wuolle et al., 1994). The participant cannot perform this task without using the system (data not shown), similar to our previous studies (Schwemmer et al., 2018; Colachis et al., 2018). The participant has motor control of his shoulder. This is used to indirectly guide and align his hand during the task. The participant was first cued to position his hand around the object (Figure 5B, cue at 0 s) and then generate motor intention to activate FES, initiate hand grasp, and transfer the object. The touch decoder always preceded the motor decoder and was time locked to object touch (Figure 5B; Video S2). The touch decoder was originally tested using a range of controls (see Figure 4 results). The assessments here extend these findings, demonstrating that the touch decoder is not significantly impacted by neural activity from simultaneous movement intention events.

Sensorimotor demultiplexing BCI control was next enabled using the simultaneous decoding of touch events and motor intention during a set of upper-limb assessments. This closed-loop demultiplexing BCI system enabled significant improvements in sense of agency (Figure 5C; $t(46) = 3$, $p = 0.004$), motor decoder latency (Figure 5D, left; $t(148) = 2.9$, $p = 0.003$), and object transfer time (Figure 5D, right; $t(148) = 2.1$, $p = 0.03$) (Figure S5: exemplary decoder inputs and outputs), compared to a motor-only BCI control. Therefore, rapid closed-loop sensory feedback not only augments sensory function but also augments motor function. Furthermore, these results provide substantial evidence that sensory feedback during movement can enhance the sense of agency and other correlates of enhanced sensorimotor integration in patients with upper-limb dysfunction (Collinger et al., 2018; Darie et al., 2017; Bensmaia and Miller, 2014; Ackerley and Kavounoudias, 2015; Marasco et al., 2018; Flesher et al., 2016, 2017, 2019). Overall, successful sensorimotor demultiplexing occurred on 100% of task trials (198 total trials). These findings demonstrate a BCI system that simultaneously demultiplexes afferent and efferent activity from human cortex for controlling multiple assistive devices and enhancing function.

## Afferent Grip-Intensity Levels Can Be Decoded from M1 to Enable Limb Reanimation Regulated by Touch

Our final set of experiments address the burden on BCI users to control moment-to-moment movement using a constant decoded motor intention. Instead of constant motor intention, touch-intensity signaling alone can potentially regulate limb reanimation during object grip. This capability could ensure appropriate BCI-mediated grip-force application, while also freeing the BCI user's attention and visual stream for other important activities.

We first assessed the hypothesis that multiple levels of afferent touch-intensity signaling from the hand could be decoded from M1 activity. Grip-force output was measured using a replicate of the standardized object with built in calibrated force sensors (see STAR Methods; grip-force levels are shown below). Three different levels of afferent touch and grip-intensity signals could be reliably decoded from M1 activity during object grip events with low false-positive rates (overall ~87 % responsiveness; Figure 6A). As expected, touch and grip-intensity decoders were not activated during control cues, which did not have touch and grip events (Figure 6A, FES Alone). Therefore, multiple levels of touch and grip intensity could be decoded from M1 activity.

As a proof-of-concept demonstration, the participant next enabled limb reanimation regulated only by decoded afferent touch and grip-intensity activity in M1 (i.e., FES solely controlled by afferent touch decoders; see STAR Methods). Trials were initiated at a high grip force (Figure 6B, Touch & High Grip trials) or a low grip force (Figure 6C, Touch & Low Grip trials) during a long duration grip of the object. Decoded Touch & High Grip served to decrease FES and grip force. Decoded Touch & Low Grip served to increase FES and grip force.

During Touch & High Grip trials (Figure 6B), grip force gradually decreased by a total of 810 g (slope test: $F = 29$, $p = 0.003$). This was mediated by a decoder-controlled decrease in FES of 1.3 mA. During Touch & Low Grip trials (Figure 6C), grip force gradually increased by a total of 120 g (slope test: $F = 19$, $p = 0.007$). This was mediated by a decoder-controlled increase in FES of 0.4 mA. As expected, touch-regulated grip

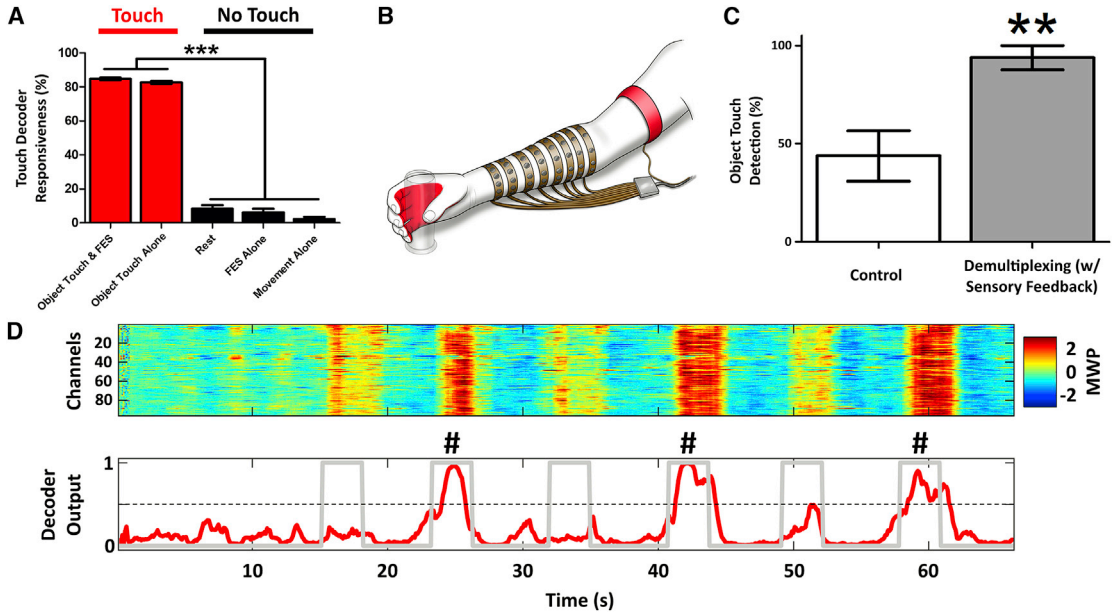


**Figure 4. Active Object Touch Can Be Decoded from M1 to Control Closed-Loop Sensory Feedback and Enhance Hand Sensory Function**

(A) Touch decoders were first assessed using "touch" or "no touch" periods (see Decoding Active Touch Alone in the STAR Methods for more details). Touch decoders had significantly higher responsiveness during object touch events (red), compared control cues lacking object touch (black) or rest (***$p<0.001$). Touch-decoder false-positive rates during cues (data not shown): Object Touch and FES = 12.2%; Object Touch Alone = 13.7%; FES Alone = 3.7%; Movement Alone = 3.3%. These results support the hypothesis that machine learning algorithms can be trained to reliably demultiplex active object touch activity from M1.

(B) Touch decoders next controlled closed-loop sensory feedback via a vibrotactile array interfaced with the sensate skin over the ipsilateral bicep (red band in the cartoon schematic).

(C) Closed-loop sensory feedback triggered by residual sensory information in M1 more than doubled object touch detection during object grip (up to ~93%) (**$p < 0.01$).

(D) Exemplary color-coded mean wavelet power (MWP) input (top) and touch-decoder outputs (bottom) during the object touch detection assessment (object placed on cue numbers 2, 4, and 6, # symbol added; cue periods = gray lines; device activation threshold = horizontal dashed line).

These results demonstrate that residual subperceptual sensory information can be demultiplexed from M1 to trigger closed-loop tactile feedback and significantly improve sensory function. Data presented are mean ± SEM.

See also Figure S4.

forces initially exhibited an adjustment period followed by a steady-state equilibration.

These results support the hypothesis that appropriate grip-force regulation can be controlled by decoded afferent touch and grip-intensity activity in M1. These results extend the sensorimotor demultiplexing BCI control results. Touch-regulated grip-intensity BCI control can be used to enable automated movement cascades while simultaneously addressing a major need of patients with SCI to use their own hand (Anderson, 2004; Snoek et al., 2004; Blabe et al., 2015). Touch-regulated grip-intensity BCI control demonstrates that limb reanimation controlled by decoded afferent cortical activity is possible. Overall, these results suggest that sensory discompleteness (Wrigley et al., 2018; Awad et al., 2015; Ioannides et al., 2002; Sabbah et al., 2002) can be leveraged for multimodal restoration of touch and motor function.

## DISCUSSION

Severe AIS-A SCI should essentially eliminate sensory information transmission to the brain that originates from skin innervated from below the lesion. Recent studies demonstrate that residual subperceptual sensory information from below the lesion is transmitted to sensory areas of the brain, even following severe clinically complete SCI (Wrigley et al., 2018; Awad et al., 2015; Ioannides et al., 2002; Sabbah et al., 2002). These results demonstrate an emerging type of SCI diagnosis—sensory discomplete. Our results extend these findings and provide electrophysiological evidence of sensory discompleteness, showing that touch-related hand sensory signals reach M1 even after AIS-A SCI. Therefore, a clinically complete SCI does not necessarily equate to an anatomically complete SCI. Our findings support the hypothesis that there is some anatomical sparing of spinal tissue even after severe AIS-A SCI, allowing sensory information transmission from below the lesion to M1, at sufficient levels for enabling sensory related BCI capabilities. Importantly, sensory discompleteness has been documented to occur in ~50% of patients with a clinically complete SCI (Wrigley et al., 2018; Finnerup et al., 2004). This study's findings have clinical applicability for sensory discomplete SCI, as well as sensory incomplete SCI. Sensory incomplete SCI may also result in residual sensory signaling from impaired dermatomes that can be used for BCI control and functional improvement.

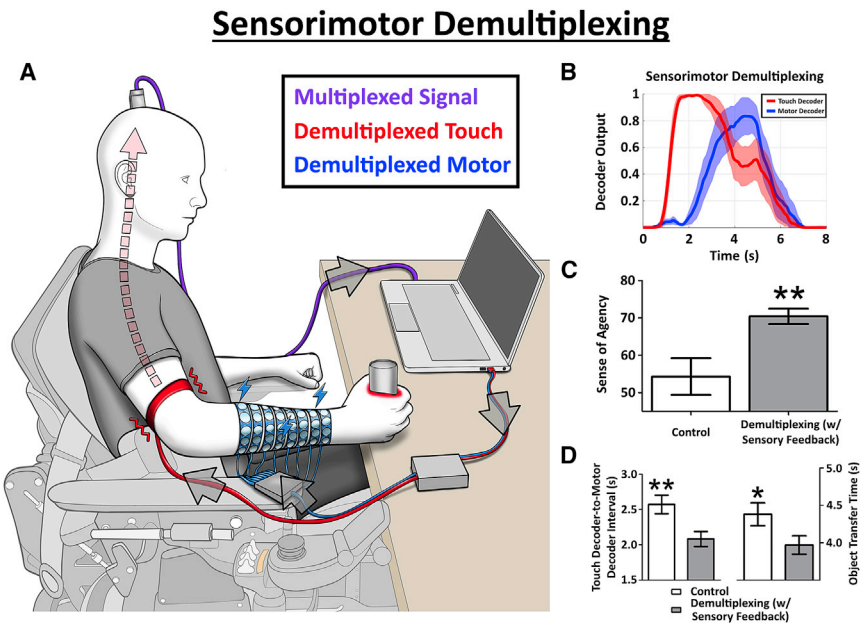


**Figure 5. Sensory and Motor Events in M1 Can Be Decoded to Enable Sensorimotor Demultiplexing BCI Control and Enhancement of Sensorimotor Function**

(A) Schematic of the participant performing a modified GRT (Wuolle et al., 1994) task with the sensorimotor demultiplexing BCI.

(B) We first challenged the touch decoder with a competing simultaneous motor decoder (during a modified GRT). As expected, touch decoders were activated before motor decoders on all object transfers (time 0 = touch cue, followed by participant-initiated motor intention; shaded bands = ± 95% confidence interval of decoder output). These results support the hypothesis that afferent touch and efferent motor intention can be simultaneously demultiplexed from M1 during upper-limb activity.

(C and D) Closed-loop sensory feedback triggered by demultiplexed sensory neural activity significantly improved the participant's sense of agency (C), motor decoder latency (D, left), and object transfer time (D, right) (average number of objects transferred per GRT assessment block: control = 9, demultiplexing with sensory feedback = 9.75).

These results demonstrate the ability to simultaneously decode afferent and efferent information from M1 and activate multiple assistive devices for augmenting sensorimotor function, constituting a sensorimotor demultiplexing BCI (*$p < 0.05$; **$p < 0.01$). Data presented are mean ± SEM.

See also Figure S5.

We also chose to use the participant's natural remaining sensory circuitry for object touch decoding and address the need of patients with SCI to use their own hand during upper-limb activity (Anderson, 2004; Snoek et al., 2004; Blabe et al., 2015). Previous surveys have documented that systems are unlikely to be used by participants if they are unreliable or difficult to use (Wielandt et al., 2006). The residual sensory signals used in the study are rapid, reliable, and arrive from the participant's hand, obviating the need for an additional device setup. Nonetheless, using a participant's hand is significantly challenging, due to the impact of severe SCI on touch transducing systems, and the approach of simultaneously demultiplexing touch and movement intention signaling. There are likely additional signal types encoded in M1, beyond motor intention and touch-related sensory information. In the future, we hope this set of findings will enable patients with an implanted BCI to maximize the information encoded in the recorded neural activity for functional gains. Overall, these findings demonstrate a BCI capable of leveraging sensory discompleteness, for simultaneously restoring both the sense of touch and motor function.

BCIs are emerging as a means to treat patients suffering from an array of functional deficits (Lebedev and Nicolelis, 2017; Hochberg et al., 2012; Collinger et al., 2013; Gilja et al., 2015; Simeral et al., 2011; Jarosiewicz et al., 2015; Bockbrader et al., 2018; Moxon and Foffani, 2015; Bouton et al., 2016; Friedenberg et al., 2017; Sharma et al., 2016; Skomrock et al., 2018; Schwemmer et al., 2018; Colachis et al., 2018; Ajiboye et al., 2017; Bockbrader et al., 2019). Accurately and consistently decoding a single device control signal is a significant challenge for BCIs. Here we extend capabilities of BCI technology to simultaneously decipher multiplexed (Akam and Kullmann, 2014) afferent and efferent neural activity or multiple levels of touch and grip intensity, for dynamically controlling motor and sensory augmentation devices. Our results support the hypothesis that subperceptual residual neural information can be reliably decoded from the human brain, and used to augment function.

## Restoring the Sense of Touch Using Residual Sensory Signals and BCI Control

The function restored to the participant using the sensorimotor demultiplexing BCI was significant in several sensorimotor functional domains, ranging from the cognitive control of hand function (Synofzik et al., 2008) to sensorimotor integration. Our control condition throughout all sensorimotor demultiplexing assessments was the participant operating the BCI system using only motor control (Figure 5). This control condition is essentially the most challenging control condition possible under the current experimental design. We therefore have designed all experiments to maximally challenge any measured functional improvements during sensorimotor demultiplexing BCI control. Nonetheless, the effect sizes are robust for the functional gains during sensorimotor demultiplexing BCI control. These gains range from an over a 100% improvement to a significant ~0.5 s increase in BCI system speed and subsequent upper-limb sensorimotor capability. We hypothesize that even larger improvements can be achieved when assessing additional functions in the absence of visual feedback. Closed-loop tactile feedback and touch-regulated grip intensity can mitigate the reliance of BCI users on visually attending to the state of the hand during movement. This would free the user's visual stream for other important functions during upper-limb activity. For example, sensorimotor demultiplexing and touch-regulated grip intensity control modes should enable increased BCI operation safety during multitasking, via notifying the user that an object has

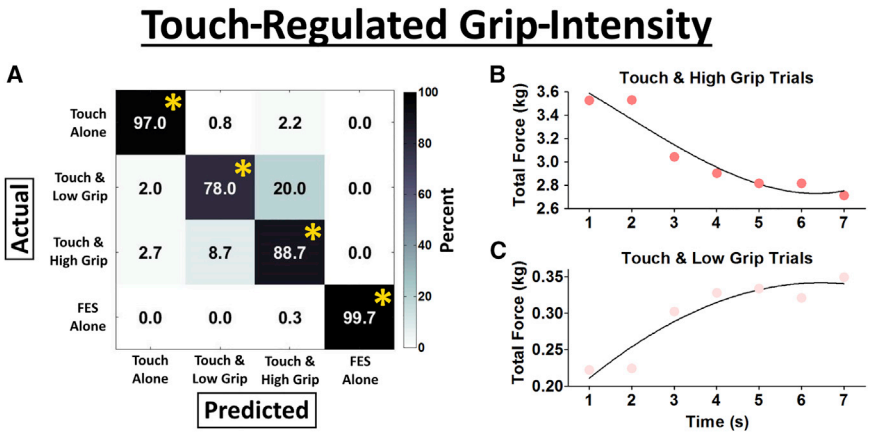


**Figure 6. Afferent Grip-Intensity Levels Can Be Decoded from M1 To Enable Limb Reanimation Regulated by Touch**

The participant also utilized touch-regulated grip-intensity BCI control, where limb reanimation is solely controlled by multiple levels of decoded touch activity.

(A) Three different levels of afferent touch and grip intensity could be reliably decoded with significant sensitivity above chance and low false-positive rates (i.e., Touch Alone, Touch & Low Grip, and Touch & High Grip; confusion matrix shows color-coded decoder response values, units = percentage; *significantly above chance at $p < 0.001$). Little to no responses occurred during control cues lacking object touch and grip (FES Alone). As a proof-of-concept demonstration, the participant next enabled touch-regulated grip-intensity BCI control, where decoded touch and grip intensity controlled limb reanimation (see Touch-Regulated Grip Intensity in the STAR Methods). Trials were started at either a high or low grip-force level during a long duration grip of the object.

(B) Decoded Touch & High Grip decreased FES and grip force in real time.

(C) Decoded Touch & Low Grip increased FES and grip force in real time. As expected, grip force initially adjusted and then equilibrated, demonstrating grip adjustment regulated by decoded afferent touch and grip-intensity levels in M1 (trends shown via polynomial fit, black lines in Figures 6B and 6C).

slipped from his or her grasp or enabling visual attention to other stimuli, other than the hand, during activities of daily living.

Due to the clinically complete cervical SCI, the participant's hand is almost completely insensate. Nonetheless, touch-related sensory information from completely insensate digits reaches M1 from critical dermatomes needed for almost all hand grasps. Therefore, electrophysiological activity mediated by sensory discompleteness significantly contributes to hand grasps during either sensorimotor demultiplexing or touch-regulated grip intensity BCI control activities. It should be noted that half of the participant's thumb has some residual abnormal sensation. Regardless, grip event detection involving multiple digits involved either guessing (at chance level) or the complete inability to recognize object grip events (Figure S1B). Together, these results support the hypothesis that both grip events and tactile stimuli to single skin locations can be subperceptual.

It is likely that sensory stimulation to dermatomes even more caudal to the SCI location can also be detected during BCI operation and leveraged for functional benefit. Previous studies demonstrate significant cortical modulation following leg or foot sensory stimulation, many spinal levels below a clinically complete cervical, thoracic, or lumbar SCI (Wrigley et al., 2018; Awad et al., 2015; Ioannides et al., 2002; Sabbah et al., 2002). This potential residual sensory activity from the lower limbs can be leveraged for improvement in future lower limb BCI technologies (Borton et al., 2014; Capogrosso et al., 2016).

## Sensorimotor Cortical Representations in the Context of Sensory Discomplete SCI

Several studies have contributed immensely to our current understanding of the sensory and motor cortex (for review, see Harding-Forrester and Feldman, 2018; Geyer et al., 2012). While there is preclinical evidence of an overlap between touch and movement representations in the cortex before injury, several studies of human cortex provide significant evidence of a separation between touch and movement representations (Harding-Forrester and Feldman, 2018; Kaas, 2012; Goldring and Ratcheson, 1972; Roux et al., 2018; Ibáñez et al., 1995; Stippich et al., 1999; Kurth et al., 1998). Importantly, SCI, and specifically clinically complete SCI, has a dramatic impact on sensory and motor cortical representations.

Severe SCI can largely "disconnect" the sensory cortex and motor cortex from their respective target tissues in the periphery, disrupting any existing sensory and motor cortical overlap. Many reports provide extensive evidence that SCI alone affects numerous attributes of sensory and motor cortical representations (for review, see Moxon et al., 2014; Mohammed and Hollis, 2018; Urbin et al., 2019). Following SCI and training, these factors can be significantly modulated, implicating cortical plasticity processes and use dependent cortical reorganization (for review, see Moxon et al., 2014; Mohammed and Hollis, 2018; Urbin et al., 2019). Importantly, BCI operation is at times also associated with significant changes in the cortex (for review, see Orsborn and Carmena, 2013; see also Sadtler et al., 2014).

A cohort of clinical studies has extended our understanding of the cortex to the context of clinically complete SCI, using a variety of cortical mapping techniques. These studies provide important evidence for sensory discompleteness—where no clinical evidence of fiber tract function is detectable, but spared fibers may affect some physiological activity (Wrigley et al., 2018; Awad et al., 2015; Ioannides et al., 2002; Sabbah et al., 2002). In the current study, we leverage sensory discompleteness for restoring the sense of touch and a variety of functional gains. One of the first examinations of supraspinal activity during sensory discomplete states was performed by Sabbah et al. in 2002. This set of investigations utilized functional magnetic resonance imaging (fMRI) of cortical structures in several patients, years after clinically complete thoracic or lumbar SCI (Sabbah et al., 2002). Sabbah et al. demonstrated that, in the absence of visual feedback, passive stimulation of the toes that the patient cannot feel activates the cortex posterior to the central sulcus in a subset of subjects. Ioannides et al. utilized

magnetoencephalography (MEG) mapping of cortical structures in patients, years after clinically complete thoracic SCI (Ioannides et al., 2002). This study showed that electro-tactile stimulation of the insensate foot evoked time-locked cortical MEG signaling again in the cortex posterior to the central sulcus in a subset of patients. In 2015, Awad et al. performed a study using fMRI of cortical structures in a subject decades after a clinically complete cervical SCI (Awad et al., 2015). Their findings show that subperceptual tactile stimulation to the lower extremities evokes fMRI signaling in the post-central somatosensory cortical modules. Last, Wrigley et al. recently demonstrated that subperceptual tactile stimulation evokes time-locked fMRI signaling in the post-central somatosensory cortex in 11 of 23 subjects with a clinically complete thoracic SCI (Wrigley et al., 2018). A small contingent of ascending fibers in the spinal cord may be involved in these findings, including the dorsal column and spinothalamic pathways. Together, these results demonstrate that subperceptual somatosensory signaling can reach cortical networks after a clinically complete SCI. Our findings extend these important clinical studies, demonstrating intracortical electrophysiological evidence of sensory discompleteness. Overall, our results support the hypothesis that this residual subperceptual signaling can be decoded and leveraged by a BCI, even in challenging active states during limb reanimation.

### Types of Sensory Feedback and Implications for BCI Implant Locations

This study uses closed-loop vibrotactile feedback during BCI operation. There are alternative ways to provide sensory feedback following SCI, including intracortical microstimulation (Flesher et al., 2016, 2017, and 2019; Armenta Salas et al., 2018; Collinger et al., 2018; Darie et al., 2017; Bensmaia and Miller, 2014; Godlove et al., 2014) or extracortical microstimulation in S1 (Caldwell et al., 2019; Johnson et al., 2013). Compared to stimulation in S1, previous studies demonstrate that tactile-based feedback enables rapid sensory perception at a significantly faster latency (Caldwell et al., 2019; Godlove et al., 2014). This was a significant contributor to the choice of using vibrotactile feedback in the current study.

BCI electrode arrays for treating upper-limb motor dysfunction are almost exclusively implanted to decode motor intention signals alone (Lebedev and Nicolelis, 2017; Hochberg et al., 2012; Collinger et al., 2013; Gilja et al., 2015; Simeral et al., 2011; Jarosiewicz et al., 2015; Bockbrader et al., 2018; Bouton et al., 2016; Friedenberg et al., 2017; Sharma et al., 2016; Skomrock et al., 2018; Schwemmer et al., 2018; Colachis et al., 2018; Ajiboye et al., 2017; Bockbrader et al., 2019). The sensorimotor demultiplexing capability can impact how BCI electrode array implant locations are determined, for interfaces seeking to decode multiplexed information classes relevant for BCI control. It will be critical to perform multimodal pre-surgical brain mapping to localize these relevant neural representations and further inform electrode array implant location. For example, seemingly small areas of the nervous system may simultaneously encode multiplexed (Akam and Kullmann, 2014) classes of sensory, motor, and contextual information relevant for next-generation neural interfaces and context adapting sensorimotor therapeutics. We anticipate future efforts that maximize information extraction from neural data and significantly increase the capability neural interfaces. Furthermore, the data presented here are from a neural interface that has been implanted for over 5 years (at the time of this writing). Reliable next-generation neural interfaces will also need to function for many years to mediate long-term benefits in patients (Zhang et al., 2018; Downey et al., 2018).

The human cortex is generally modular and can encode a variety of stimuli or other activity. The sensory signal utilized in this study may arrive in M1 directly, from a separate source via corticocortical transmission and propagating activity, or both (Takahashi et al., 2011; Rubino et al., 2006). Additional studies are required to further understand the contribution of the neighboring somatosensory cortical modules and subcortical structures to the M1 activity observed in the current study. Nonetheless, evidence is accumulating that M1, and other cortical modules, encode a multiplicity of features related to experience beyond their primary processing designation (Hatsopoulos and Suminski, 2011; Suminski et al., 2010; Shaikhouni et al., 2013; Hari et al., 1998; Schroeder et al., 2017; Manohar et al., 2017; Ganzer et al., 2013, 2016). For future BCI applications, an array of powerful control signals can potentially be demultiplexed from a single recording site, or multiple distributed interfaces. Advanced decoding strategies (Schwemmer et al., 2018) may be needed to decipher the multitude of representations encoded in neural activity and further enable demultiplexing BCIs. Regardless, the results we present here are a step toward the design of next-generation neural interfaces capable of demultiplexing multimodal neural information for distributed device control and functional improvement.

## STAR★METHODS

Detailed methods are provided in the online version of this paper and include the following:

- KEY RESOURCES TABLE
- RESOURCE AVAILABILITY
  - Lead Contact
  - Materials Availability
  - Data and Code Availability
- EXPERIMENTAL MODEL AND SUBJECT DETAILS
  - Study Participant
- METHOD DETAILS
  - Neural Recording System
  - Neural Signal Conditioning
  - Decoding Using Support Vector Machines
  - FES system
- QUANTIFICATION AND STATISTICAL ANALYSIS
- ADDITIONAL RESOURCES

### SUPPLEMENTAL INFORMATION

Supplemental Information can be found online at https://doi.org/10.1016/j.cell.2020.03.054.

### ACKNOWLEDGMENTS

We would like to thank the study participant for his contributions and exceptional dedication to the ongoing clinical study and technology development.

We would also like to thank our development and management teams at Battelle Memorial Institute, Nathan Platfoot and Nick Annetta for helping construct the sensory feedback interface electronics, Jake Pyzza and Josh Branch for helping build the standardized grip-force measurement object, Russ Kittel for his contributions to the manuscript graphics, and several Battelle team members who contributed to the preparation and review of the manuscript. A special thanks to Dr. Keith Tansey for his manuscript reviews and critical insights regarding the clinical importance of these findings. Financial support for this study came from Battelle Memorial Institute and The Ohio State University Department of Physical Medicine & Rehabilitation. M.A.B. also acknowledges the invaluable mentorship of the Rehabilitation Medicine Scientist Training Program at the Association of Academic Physiatrists.

## AUTHOR CONTRIBUTIONS

P.D.G., S.C.C., M.A.S., M.A.B., D.A.F., and C.F.D. conceived and designed the experiments. P.D.G., S.C.C., C.E.S., M.A.B., A.F.J., and C.F.D. performed the experiments and analysis. P.D.G., D.J.W., and G.S. provided project supervision. All authors contributed to writing and editing the manuscript.

## DECLARATION OF INTERESTS

The authors declare competing interests, as they are employed by institutions that provided the funding for this work and/or have filed associated patents. P.D.G., S.C.C., M.A.S., D.A.F., C.F.D., C.E.S., A.F.J., and G.S. were all employed by Battelle Memorial Institute at the time of this study. D.J.W. was a consultant for Battelle Memorial Institute at the time of this study. M.A.B. is employed by the Ohio State University. D.A.F. and G.S. are listed as inventors on the United States patent application US 2018/0178008 (related WO 2016/196797), and G.S. is listed as an inventor on the United States patent application US 2015/0306373. These are related to the neural bridging BCI technology and stimulation interface used in the paper.

Received: April 11, 2019
Revised: October 9, 2019
Accepted: March 24, 2020
Published: April 16, 2020

## REFERENCES

Ackerley, R., and Kavounoudias, A. (2015). The role of tactile afference in shaping motor behaviour and implications for prosthetic innovation. Neuropsychologia *79*, 192–205.

Ajiboye, A.B., Willett, F.R., Young, D.R., Memberg, W.D., Murphy, B.A., Miller, J.P., Walter, B.L., Sweet, J.A., Hoyen, H.A., Keith, M.W., et al. (2017). Restoration of reaching and grasping movements through brain-controlled muscle stimulation in a person with tetraplegia: a proof-of-concept demonstration. Lancet *389*, 1821–1830.

Akam, T., and Kullmann, D.M. (2014). Oscillatory multiplexing of population codes for selective communication in the mammalian brain. Nat. Rev. Neurosci. *15*, 111–122.

Anderson, K.D. (2004). Targeting recovery: priorities of the spinal cord-injured population. J. Neurotrauma *21*, 1371–1383.

Annetta, N.V., Friend, J., Schimmoeller, A., Buck, V.S., Friedenberg, D.A., Bouton, C.E., Bockbrader, M.A., Ganzer, P.D., Colachis Iv, S.C., Zhang, M., et al. (2019). A High Definition Noninvasive Neuromuscular Electrical Stimulation System for Cortical Control of Combinatorial Rotary Hand Movements in a Human With Tetraplegia. IEEE Trans. Biomed. Eng. *66*, 910–919.

Armenta Salas, M., Bashford, L., Kellis, S., Jafari, M., Jo, H., Kramer, D., Shanfield, K., Pejsa, K., Lee, B., Liu, C.Y., and Andersen, R.A. (2018). Proprioceptive and cutaneous sensations in humans elicited by intracortical microstimulation. eLife *7*, 1–11.

Awad, A., Levi, R., Lindgren, L., Hultling, C., Westling, G., Nyberg, L., and Eriksson, J. (2015). Preserved somatosensory conduction in a patient with complete cervical spinal cord injury. J. Rehabil. Med. *47*, 426–431.

Bensmaia, S.J., and Miller, L.E. (2014). Restoring sensorimotor function through intracortical interfaces: progress and looming challenges. Nat. Rev. Neurosci. *15*, 313–325.

Blabe, C.H., Gilja, V., Chestek, C.A., Shenoy, K.V., Anderson, K.D., and Henderson, J.M. (2015). Assessment of brain-machine interfaces from the perspective of people with paralysis. J. Neural Eng. *12*, 043002.

Bockbrader, M.A., Francisco, G., Lee, R., Olson, J., Solinsky, R., and Boninger, M.L. (2018). Brain Computer Interfaces in Rehabilitation Medicine. PM&R *10*, S233–S243.

Bockbrader, M., Annetta, N., Friedenberg, D., Schwemmer, M., Skomrock, N., Colachis, S., 4th, Zhang, M., Bouton, C., Rezai, A., Sharma, G., and Mysiw, W.J. (2019). Clinically significant gains in skillful grasp coordination by an individual with tetraplegia using an implanted brain-computer interface with forearm transcutaneous muscle stimulation. Arch. Phys. Med. Rehabil. *100*, 30163–30167.

Borton, D., Bonizzato, M., Beauparlant, J., DiGiovanna, J., Moraud, E.M., Wenger, N., Musienko, P., Minev, I.R., Lacour, S.P., Millán, Jdel.R., et al. (2014). Corticospinal neuroprostheses to restore locomotion after spinal cord injury. Neurosci. Res. *78*, 21–29.

Bouton, C.E., Shaikhouni, A., Annetta, N.V., Bockbrader, M.A., Friedenberg, D.A., Nielson, D.M., Sharma, G., Sederberg, P.B., Glenn, B.C., Mysiw, W.J., et al. (2016). Restoring cortical control of functional movement in a human with quadriplegia. Nature *533*, 247–250.

Caldwell, D.J., Cronin, J.A., Wu, J., Weaver, K.E., Ko, A.L., Rao, R.P.N., and Ojemann, J.G. (2019). Direct stimulation of somatosensory cortex results in slower reaction timescompared to peripheral touch in humans. Sci. Rep. *9*, 1–11.

Capogrosso, M., Milekovic, T., Borton, D., Wagner, F., Moraud, E.M., Mignardot, J.B., Buse, N., Gandar, J., Barraud, Q., Xing, D., et al. (2016). A brain-spine interface alleviating gait deficits after spinal cord injury in primates. Nature *539*, 284–288.

Chatterjee, A., Aggarwal, V., Ramos, A., Acharya, S., and Thakor, N.V. (2007). A brain-computer interface with vibrotactile biofeedback for haptic information. J. Neuroeng. Rehabil. *4*, 40.

Chang, C.C., and Lin, C.J. (2011). LIBSVM: a library for support vector machines. (ACM Transactions on Intelligent Systems and Technology), pp. 2:27:1–27:27, Software available at. https://www.csie.ntu.edu.tw/~cjlin/libsvm.

Colachis, S.C., 4th, Bockbrader, M.A., Zhang, M., Friedenberg, D.A., Annetta, N.V., Schwemmer, M.A., Skomrock, N.D., Mysiw, W.J., Rezai, A.R., Bresler, H.S., and Sharma, G. (2018). Dexterous Control of Seven Functional Hand Movements Using Cortically-Controlled Transcutaneous Muscle Stimulation in a Person With Tetraplegia. Front. Neurosci. *12*, 208.

Collinger, J.L., Wodlinger, B., Downey, J.E., Wang, W., Tyler-Kabara, E.C., Weber, D.J., McMorland, A.J., Velliste, M., Boninger, M.L., and Schwartz, A.B. (2013). High-performance neuroprosthetic control by an individual with tetraplegia. Lancet *381*, 557–564.

Collinger, J.L., Gaunt, R.A., and Schwartz, A.B. (2018). Progress towards restoring upper limb movement and sensation through intracortical brain-computer interfaces. Curr. Opin. Biomed. Eng. *8*, 84–92.

Darie, R., Powell, M., and Borton, D. (2017). Delivering the Sense of Touch to the Human Brain. Neuron *93*, 728–730.

Dimitrijevic, M.R. (1987). Neurophysiology in spinal cord injury. Paraplegia *25*, 205–208.

Downey, J.E., Schwed, N., Chase, S.M., Schwartz, A.B., and Collinger, J.L. (2018). Intracortical recording stability in human brain-computer interface users. J. Neural Eng. *15*, 046016.

Finnerup, N.B., Gyldensted, C., Fuglsang-Frederiksen, A., Bach, F.W., and Jensen, T.S. (2004). Sensory perception in complete spinal cord injury. Acta Neurol. Scand. *109*, 194–199.

Flesher, S.N., Collinger, J.L., Foldes, S.T., Weiss, J.M., Downey, J.E., Tyler-Kabara, E.C., Bensmaia, S.J., Schwartz, A.B., Boninger, M.L., and Gaunt,

R.A. (2016). Intracortical microstimulation of human somatosensory cortex. Sci. Transl. Med. *8*, 361ra141.

Flesher, S.N., Downey, J., Collinger, J., Foldes, S., Weiss, J., Tyler-Kabara, E., Bensmaia, S., Schwartz, A., Boninger, M., and Gaunt, R. (2017). Intracortical microstimulation as a feedback source forbrain-computer interface users. In Brain-Computer Interface Research. Springer Briefs in Electrical and Computer Engineering, C. Guger, B. Allison, and M. Lebedev, eds. (Springer), pp. 43–54.

Flesher, S.N., Downey, J.E., Weiss, J.M., Hughes, C.L., Herrera, A.J., Tyler-Kabara, E.C., Boninger, M.L., Collinger, J.L., and Gaunt, R.A. (2019). Restored tactile sensation improves neuroprosthetic arm control. bioRxiv. https://doi.org/10.1101/653428.

Friedenberg, D.A., Bouton, C.E., Annetta, N.V., Skomrock, N., Mingming Zhang, Schwemmer, M., Bockbrader, M.A., Mysiw, W.J., Rezai, A.R., Bresler, H.S., and Sharma, G. (2016). Big data challenges in decoding cortical activity in a human with quadriplegia to inform a brain computer interface. Conf. Proc. IEEE Eng. Med. Biol. Soc. *2016*, 3084–3087.

Friedenberg, D.A., Schwemmer, M.A., Landgraf, A.J., Annetta, N.V., Bockbrader, M.A., Bouton, C.E., Zhang, M., Rezai, A.R., Mysiw, W.J., Bresler, H.S., and Sharma, G. (2017). Neuroprosthetic-enabled control of graded arm muscle contraction in a paralyzed human. Sci. Rep. *7*, 8386.

Ganzer, P.D., Moxon, K.A., Knudsen, E.B., and Shumsky, J.S. (2013). Serotonergic pharmacotherapy promotes cortical reorganization after spinal cord injury. Exp. Neurol. *241*, 84–94.

Ganzer, P.D., Manohar, A., Shumsky, J.S., and Moxon, K.A. (2016). Therapy induces widespread reorganization of motor cortex after complete spinal transection that supports motor recovery. Exp. Neurol. *279*, 1–12.

Geyer, S., Luppino, G., and Rozzi, S. (2012). Motor cortex. In The Humannervous System, J. Mai and G. Paxinos, eds. (Elsevier), pp. 1074–1109.

Gilja, V., Pandarinath, C., Blabe, C.H., Nuyujukian, P., Simeral, J.D., Sarma, A.A., Sorice, B.L., Perge, J.A., Jarosiewicz, B., Hochberg, L.R., et al. (2015). Clinical translation of a high-performance neural prosthesis. Nat. Med. *21*, 1142–1145.

Godlove, J.M., Whaite, E.O., and Batista, A.P. (2014). Comparing temporal aspects of visual, tactile, and microstimulation feedback for motor control. J. Neural Eng. *11*, 046025.

Goldring, S., and Ratcheson, R. (1972). Human motor cortex: sensory input data from single neuron recordings. Science *175*, 1493–1495.

Harding-Forrester, S., and Feldman, D.E. (2018). Somatosensory maps. Handb. Clin. Neurol. *151*, 73–102.

Hari, R., Forss, N., Avikainen, S., Kirveskari, E., Salenius, S., and Rizzolatti, G. (1998). Activation of human primary motor cortex during action observation: a neuromagnetic study. Proc. Natl. Acad. Sci. USA *95*, 15061–15065.

Hatsopoulos, N.G., and Suminski, A.J. (2011). Sensing with the motor cortex. Neuron *72*, 477–487.

Hochberg, L.R., Bacher, D., Jarosiewicz, B., Masse, N.Y., Simeral, J.D., Vogel, J., Haddadin, S., Liu, J., Cash, S.S., van der Smagt, P., and Donoghue, J.P. (2012). Reach and grasp by people with tetraplegia using a neurally controlled robotic arm. Nature *485*, 372–375.

Ibáñez, V., Deiber, M.P., Sadato, N., Toro, C., Grissom, J., Woods, R.P., Mazziotta, J.C., and Hallett, M. (1995). Effects of stimulus rate on regional cerebral blood flow after median nerve stimulation. Brain *118*, 1339–1351.

Ioannides, A.A., Liu, L., Khurshudyan, A., Bodley, R., Poghosyan, V., Shibata, T., Dammers, J., and Jamous, A. (2002). Brain activation sequences following electrical limb stimulation of normal and paraplegic subjects. Neuroimage *16*, 115–129.

Jarosiewicz, B., Sarma, A.A., Bacher, D., Masse, N.Y., Simeral, J.D., Sorice, B., Oakley, E.M., Blabe, C., Pandarinath, C., Gilja, V., et al. (2015). Virtual typing by people with tetraplegia using a self-calibrating intracortical brain-computer interface. Sci. Transl. Med. *7*, 313ra179.

Johansson, R.S., and Flanagan, J.R. (2009). Coding and use of tactile signals from the fingertips in object manipulation tasks. Nat. Rev. Neurosci. *10*, 345–359.

Johnson, L.A., Wander, J.D., Sarma, D., Su, D.K., Fetz, E.E., and Ojemann, J.G. (2013). Direct electrical stimulation of the somatosensory cortex in humans using electrocorticography electrodes: a qualitative and quantitative report. J. Neural Eng. *10*, 036021.

Kaas, J.H. (2012). Somatosensory system. In The Human Nervous System, J. Mai and G. Paxinos, eds. (Elsevier), pp. 1074–1109.

Kalra, M., Rakheja, S., Marcotte, P., Dewangan, K.N., and Adewusi, S. (2015). Measurement of coupling forces at the power tool handle-hand interface. Int. J. Ind. Ergon. *50*, 105–120.

Kalsi-Ryan, S., Curt, A., Verrier, M.C., and Fehlings, M.G. (2012). Development of the Graded Redefined Assessment of Strength, Sensibility and Prehension (GRASSP): reviewing measurement specific to the upper limb in tetraplegia. J. Neurosurg. Spine *17* (1, Suppl), 65–76.

Kao, K., Huang, J., and Pan, M. (2014). Design and Implementation of Assistive Devices for Poststroke Rehabilitation of Hand and Fingers. J. Med. Device. *8*, 020933.

Kirshblum, S.C., Burns, S.P., Biering-Sorensen, F., Donovan, W., Graves, D.E., Jha, A., Johansen, M., Jones, L., Krassioukov, A., Mulcahey, M.J., et al. (2011). International standards for neurological classification of spinal cord injury (revised 2011). J. Spinal Cord Med. *34*, 535–546.

Kirshblum, S.C., Biering-Sorensen, F., Betz, R., Burns, S., Donovan, W., Graves, D.E., Johansen, M., Jones, L., Mulcahey, M.J., Rodriguez, G.M., et al. (2014). International Standards for Neurological Classification of Spinal Cord Injury: cases with classification challenges. J. Spinal Cord Med. *37*, 120–127.

Kumar, N., Manjaly, J.A., and Miyapuram, K.P. (2014). Feedback about action performed can alter the sense of self-agency. Front. Psychol. *5*, 145.

Kurth, R., Villringer, K., Mackert, B.M., Schwiemann, J., Braun, J., Curio, G., Villringer, A., and Wolf, K.J. (1998). fMRI assessment of somatotopy in human Brodmann area 3b by electrical finger stimulation. Neuroreport *9*, 207–212.

Lebedev, M.A., and Nicolelis, M.A.L. (2017). Brain-Machine Interfaces: From Basic Science to Neuroprostheses and Neurorehabilitation. Physiol. Rev. *97*, 767–837.

Lee, M.W., McPhee, R.W., and Stringer, M.D. (2008). An evidence-based approach to human dermatomes. Clin. Anat. *21*, 363–373.

Manohar, A., Foffani, G., Ganzer, P.D., Bethea, J.R., and Moxon, K.A. (2017). Cortex-dependent recovery of unassisted hindlimb locomotion after complete spinal cord injury in adult rats. eLife *6*, e23532.

Marasco, P.D., Hebert, J.S., Sensinger, J.W., Shell, C.E., Schofield, J.S., Thumser, Z.C., Nataraj, R., Beckler, D.T., Dawson, M.R., Blustein, D.H., et al. (2018). Illusory movement perception improves motor control for prosthetic hands. Sci. Transl. Med. *10*, eaao6990.

Meek, S.G., Jacobsen, S.C., and Goulding, P.P. (1989). Extended physiologic taction: design and evaluation of a proportional force feedback system. J. Rehabil. Res. Dev. *26*, 53–62.

Mohammed, H., and Hollis, E.R., 2nd. (2018). Cortical Reorganization of Sensorimotor Systems and the Role of Intracortical Circuits After Spinal Cord Injury. Neurotherapeutics *15*, 588–603.

Moxon, K.A., and Foffani, G. (2015). Brain-machine interfaces beyond neuroprosthetics. Neuron *86*, 55–67.

Moxon, K.A., Oliviero, A., Aguilar, J., and Foffani, G. (2014). Cortical reorganization after spinal cord injury: always for good? Neuroscience *283*, 78–94.

Obhi, S.S., and Hall, P. (2011). Sense of agency and intentional binding in joint action. Exp. Brain Res. *211*, 655–662.

Ojala, M., and Garriga, G. (2010). Permutation tests for studying classifier performance. J. Mach. Learn. Res. *11*, 1833–1863.

Orsborn, A.L., and Carmena, J.M. (2013). Creating new functional circuits for action via brain-machine interfaces. Front. Comput. Neurosci. *7*, 157.

Patterson, P.E., and Katz, J.A. (1992). Design and evaluation of a sensory feedback system that provides grasping pressure in a myoelectric hand. J. Rehabil. Res. Dev. *29*, 1–8.

Pehlivan, A., Sergi, F., Erwin, A., and Yozbatiran, N. (2014). Design and validation of the RiceWrist-S exoskeleton for robotic rehabilitation after incomplete spinal cord injury. Rehabilitation Robotics and Human-Robot Interaction *32*, 1415–1431.

Pylatiuk, C., Kargov, A., and Schulz, S. (2006). Design and evaluation of a low-cost force feedbacksystem for myoelectric prosthetic hands. J. Prosthet. Orthot. *18*, 57–61.

Quiroga, R.Q., Nadasdy, Z., and Ben-Shaul, Y. (2004). Unsupervised spike detection and sorting with wavelets and superparamagnetic clustering. Neural Comput. *16*, 1661–1687.

Roux, F.E., Djidjeli, I., and Durand, J.B. (2018). Functional architecture of the somatosensory homunculus detected by electrostimulation. J. Physiol. *596*, 941–956.

Rubino, D., Robbins, K.A., and Hatsopoulos, N.G. (2006). Propagating waves mediate information transfer in the motor cortex. Nat. Neurosci. *9*, 1549–1557.

Sabbah, P., de, S.S., Leveque, C., Gay, S., Pfefer, F., Nioche, C., Sarrazin, J.L., Barouti, H., Tadie, M., and Cordoliani, Y.S. (2002). Sensorimotor cortical activity in patients with complete spinal cord injury: a functional magnetic resonance imaging study. J. Neurotrauma *19*, 53–60.

Sadtler, P.T., Quick, K.M., Golub, M.D., Chase, S.M., Ryu, S.I., Tyler-Kabara, E.C., Yu, B.M., and Batista, A.P. (2014). Neural constraints on learning. Nature *512*, 423–426.

Schroeder, K.E., Irwin, Z.T., Bullard, A.J., Thompson, D.E., Bentley, J.N., Stacey, W.C., Patil, P.G., and Chestek, C.A. (2017). Robust tactile sensory responses in finger area of primate motor cortex relevant to prosthetic control. J. Neural Eng. *14*, 046016.

Schwemmer, M.A., Skomrock, N.D., Sederberg, P.B., Ting, J.E., Sharma, G., Bockbrader, M.A., and Friedenberg, D.A. (2018). Meeting brain-computer interface user performance expectations using a deep neural network decoding framework. Nat. Med. *24*, 1669–1676.

Shaikhouni, A., Donoghue, J.P., and Hochberg, L.R. (2013). Somatosensory responses in a human motor cortex. J. Neurophysiol. *109*, 2192–2204.

Sharma, G., Friedenberg, D.A., Annetta, N., Glenn, B., Bockbrader, M., Majstorovic, C., Domas, S., Mysiw, W.J., Rezai, A., and Bouton, C. (2016). Using an Artificial Neural Bypass to Restore Cortical Control of Rhythmic Movements in a Human with Quadriplegia. Sci. Rep. *6*, 33807.

Sherwood, A.M., Dimitrijevic, M.R., and McKay, W.B. (1992). Evidence of subclinical brain influence in clinically complete spinal cord injury: discomplete SCI. J. Neurol. Sci. *110*, 90–98.

Simeral, J.D., Kim, S.-P., Black, M.J., Donoghue, J.P., and Hochberg, L.R. (2011). Neural control of cursor trajectory and click by a human with tetraplegia 1000 days after implant of an intracortical microelectrode array. J. Neural Eng. *8*, 025027.

Skomrock, N.D., Schwemmer, M.A., Ting, J.E., Trivedi, H.R., Sharma, G., Bockbrader, M.A., and Friedenberg, D.A. (2018). A Characterization of Brain-Computer Interface Performance Trade-Offs Using Support Vector Machines and Deep Neural Networks to Decode Movement Intent. Front. Neurosci. *12*, 763.

Snoek, G.J., IJzerman, M.J., Hermens, H.J., Maxwell, D., and Biering-Sorensen, F. (2004). Survey of the needs of patients with spinal cord injury: impact and priority for improvement in hand function in tetraplegics. Spinal Cord *42*, 526–532.

Stippich, C., Hofmann, R., Kapfer, D., Hempel, E., Heiland, S., Jansen, O., and Sartor, K. (1999). Somatotopic mapping of the human primary somatosensory cortex by fully automated tactile stimulation using functional magnetic resonance imaging. Neurosci. Lett. *277*, 25–28.

Suminski, A.J., Tkach, D.C., Fagg, A.H., and Hatsopoulos, N.G. (2010). Incorporating feedback from multiple sensory modalities enhances brain-machine interface control. J. Neurosci. *30*, 16777–16787.

Synofzik, M., Vosgerau, G., and Newen, A. (2008). I move, therefore I am: a new theoretical framework to investigate agency and ownership. Conscious. Cogn. *17*, 411–424.

Takahashi, K., Saleh, M., Penn, R.D., and Hatsopoulos, N.G. (2011). Propagating waves in human motor cortex. Front. Hum. Neurosci. *5*, 40.

Urbin, M.A., Royston, D.A., Weber, D.J., Boninger, M.L., and Collinger, J.L. (2019). What is the functional relevance of reorganization in primary motor cortex after spinal cord injury? Neurobiol. Dis. *121*, 286–295.

Wielandt, T., Mckenna, K., Tooth, L., and Strong, J. (2006). Factors that predict the post-discharge use of recommended assistive technology (AT). Disabil. Rehabil. Assist. Technol. *1*, 29–40.

Wrigley, P.J., Siddall, P.J., and Gustin, S.M. (2018). New evidence for preserved somatosensory pathways in complete spinal cord injury: A fMRI study. Hum. Brain Mapp. *39*, 588–598.

Wuolle, K.S., Doren, C.L.V., Thrope, G.B., Keith, M.W., and Peckham, P.H. (1994). Development of a quantitative hand grasp and release test for patients with tetraplegia using a hand neuroprosthesis. J. Hand Surg. *19*, 209–342.

Yozbatiran, N., Der-Yeghiaian, L., and Cramer, S.C. (2008). A standardized approach to performing the action research arm test. Neurorehabil. Neural Repair *22*, 78–90.

Zhang, M., Schwemmer, M.A., Ting, J.E., Majstorovic, C.E., Friedenberg, D.A., Bockbrader, M.A., et al. (2018). Extracting wavelet based neural features from human intracortical recordings forneuroprosthetics applications. Bioelectron. Med. *4*, 11.

# STAR★METHODS

## KEY RESOURCES TABLE

| REAGENT or RESOURCE | SOURCE | IDENTIFIER |
|---|---|---|
| Software and Algorithms | | |
| MATLAB | Mathworks | http://www.mathworks.com/ |
| LIBSVM: a library for support vector machines | Chang & Lin, 2011 | https://www.csie.ntu.edu.tw/~cjlin/libsvm |
| Wave clus | Quiroga et al., 2004 | https://github.com/csn-le/wave_clus |

## RESOURCE AVAILABILITY

### Lead Contact

Further information and requests for resources should be directed to and will be fulfilled by the Lead Contact: ganzer@battelle.org.

### Materials Availability

This study did not generate any new unique reagents.

### Data and Code Availability

Data and code used in this study can be made available to qualified individuals for collaboration provided that a written agreement is executed in advance between Battelle Memorial Institute and the requester's affiliated institution. Such inquiries or requests should be directed to the Lead Contact: ganzer@battelle.org.

## EXPERIMENTAL MODEL AND SUBJECT DETAILS

### Study Participant

Approval for this study was obtained from the US Food and Drug Administration (Investigational Device Exemption) and The Ohio State University Medical Center Institutional Review Board (Columbus, Ohio). The study met institutional requirements for the conduct of human subjects and was registered on the http://www.ClinicalTrials.gov website (identifier: NCT01997125). The participant referenced in this work completed an informed consent process before commencement of the study. The participant was either completely blinded to the experimental conditions or given brief instructions to complete the necessary actions. Cue and trial parameters were randomized as needed, detailed below.

The study participant was a 27-year-old male with stable, non-spastic C5 quadriplegia resulting from a cervical SCI. The participant had control of full bilateral elbow flexion (grade 5/5), active wrist extension with radial deviation through an incomplete range of motion against gravity (grade 2/5), but no motor function below the level of C6. His sensory level was C5 on the right (because of altered but present light touch on his thumb) and C6 on the left. His injury was clinically complete, with an overall neurological level of C5 American Spinal Injury Association Impairment Scale A (AIS-A), with zone of partial preservation for motor function to C6 bilaterally according to the International Standards for Neurological Classification of Spinal Cord Injury (Kirshblum et al., 2014).

The participant underwent implantation of a 96 channel Utah microelectrode recording array (Blackrock Microsystems, Inc.; Salt Lake, Utah) in his left primary motor cortex (Figure 1A). The hand area of motor cortex was identified preoperatively by fusing functional magnetic resonance imaging (fMRI) activation maps obtained while the patient attempted movements co-registered to the preoperative planning MRI. Full details of the fMRI and surgical procedures can be found in Bouton et al., 2016.

## METHOD DETAILS

### Neural Recording System

Neural data was acquired using a Utah microelectrode recording array (Blackrock Microsystems, Inc.; Salt Lake City, Utah) and the Neuroport neural data acquisition system. Recorded data from all 96 recording array channels was sampled at 30 kHz and band pass filtered online from 0.3 – 7.5 kHz using a third order Butterworth analog hardware filter. The neural data was then digitized and sent to a PC for saving or further on-line processing using a custom interface in MATLAB 2014a (The MathWorks; Natick, MA).

### Neural Signal Conditioning

We used stimulation artifact removal, mean wavelet power (MWP) estimation, and non-linear support vector machine (SVM) decoding, similar to our previous studies (Bouton et al., 2016; Sharma et al., 2016; Skomrock et al., 2018; Schwemmer et al., 2018; Colachis

et al., 2018; Bockbrader et al., 2019; Annetta et al., 2019). Details for MWP calculation and SVM decoding are provided in the next section. Details for stimulation artifact removal: functional electrical stimulation (FES) induced stimulation artifacts were detected by threshold crossings of 500 μV occurring simultaneously on at least 4 of 12 randomly selected channels. A 3.5 ms window of data around each detected artifact was then removed and adjacent data segments were rejoined. This approach leaves the vast majority of the neural data intact. Our series of control experiments confirm the removal of the stimulation artifact across several contexts (specifically Figures S3A and S3B; Figures 4A and 6A, FES alone). Data collected here combined with our previous studies demonstrates the robust ability to remove artifacts from the data with this approach prior to signal analysis.

### Decoding Using Support Vector Machines

Neural activity was next measured using MWP, similar to our previous studies (Bouton et al., 2016; Friedenberg et al., 2017; Sharma et al., 2016; Skomrock et al., 2018; Schwemmer et al., 2018; Colachis et al., 2018; Bockbrader et al., 2019; Annetta et al., 2019). Details for MWP calculation and SVM decoding: wavelet decomposition was applied to the raw voltage data, using the 'db4' mother wavelet and 11 wavelet scales. Wavelet scales 3–6 were used, corresponding to the multiunit frequency band spanning approximately 234 to 3,750 Hz. The mean of the wavelet coefficients for each scale of each channel was calculated every 100 ms and a 1 s wide boxcar filter was applied to smooth the data. Baseline drift in the data was estimated by using a 15 s boxcar filter and was subtracted from the smoothed mean wavelet coefficients for the corresponding 100 ms window. The mean coefficients were then standardized per channel, per scale, by subtracting the mean and dividing by the standard deviation of those scales and channels during the training blocks. The four scales were then combined by averaging the standardized coefficients for each channel, resulting in 96 MWP values, one for each electrode in the recording array, for every 100 ms of data. The resulting MWP values were used as input to the given non-linear SVM decoder (Friedenberg et al., 2016; Chang and Lin, 2011) to generate class predictions. Predictions were used to either evaluate decoder performance offline or control a given end effector device online (e.g., FES). Specific details on SVM hyperparameters or model training and testing methods are provided below for both the passive sensory stimulation or active object touch experiments.

### FES system

The FES system (either cuff-based or a sleeve) used to stimulate the arm musculature and produce movement was identical to our previous studies (Bouton et al., 2016; Friedenberg et al., 2017; Sharma et al., 2016; Skomrock et al., 2018; Schwemmer et al., 2018; Colachis et al., 2018; Bockbrader et al., 2019; Annetta et al., 2019). Details for the FES system: the cuff-based FES system consists of a multi-channel stimulator and a flexible cuff containing 130 electrodes that is wrapped around the participant's forearm. During use, hydrogel disks (Axelgaard; Fallbrook, CA) were placed between the electrodes and skin to act as a conduction enhancer. The electrodes are 12 mm in diameter and were spaced at 22 mm intervals along the longitudinal axis of the forearm and 15 mm intervals in the transverse direction. Current-controlled, monophasic rectangular pulses (50 Hz pulse rate and 500 μs pulse width) were used to provide electrical stimulation and produce movement. Pulse amplitudes ranged from 0 to 20 mA and were updated every 100 ms. Stimulator calibrations were performed for a given movement using an anatomy-based trial-and-error method to determine appropriate electrode spatial patterns.

All methods below are separated into either passive sensory stimulation or active object touch experiments. All experiments were performed across a total of approximately 1.75 years.

#### *Passive Sensory Stimulation Experiments*

*Passive Sensory Stimulation.*

We first assessed evoked neural activity in left primary motor cortex M1 using bi-polar electro-tactile stimulation at skin locations on the participant's arm and hand. Electro-tactile stimulation was chosen for several reasons: 1) its use in our previous FES studies (Bouton et al., 2016; Friedenberg et al., 2017; Sharma et al., 2016; Skomrock et al., 2018; Schwemmer et al., 2018; Colachis et al., 2018; Bockbrader et al., 2019; Annetta et al., 2019); 2) its safety and precise electronic control of stimulus timing and intensity; and 3) its ability to evoke activity in M1 following from our pilot recordings. We targeted 4 skin locations innervated by the spinal cord above, at, and below the participant's C5 SCI (Figure S1C). The skin stimulation was performed at the following dermatomes (Kalsi-Ryan et al., 2012; Lee et al., 2008):

1. C5 dermatome (forearm; electrode locations: skin above the extensor carpi radialis longus)
2. C6 dermatome (thumb; electrode locations: skin above the distal phalanx of digit 1)
3. C6 / C7 dermatome (index; electrode locations: skin above the distal phalanx of digit 2)
4. C7 / C8 dermatome (middle; electrode locations: skin above the distal phalanx of digit 3)

Forearm, thumb, index, and middle are used to describe these 4 skin stimulation sites throughout the manuscript. A subset of control recordings were also performed on the opposite arm ipsilateral to the M1 implant for the homotopic thumb and forearm locations at the maximum stimulation intensity (Figure S3). Cutaneous landmarks and/or ink markings were used throughout as needed to confirm skin stimulation locations. The participant wore an eye mask and ear plugs during all passive sensory stimulation experiments to significantly reduce any external visual and auditory events during recordings. Passive sensory recordings were also video recorded and performed under the supervision of a licensed physiatrist.

The stimulation interface for a given skin location consisted of a pair of hydrogel disk electrodes adhered to a modified version of the FES interface used in our previous studies (Bouton et al., 2016; Friedenberg et al., 2017; Sharma et al., 2016; Skomrock et al., 2018; Schwemmer et al., 2018; Colachis et al., 2018; Bockbrader et al., 2019; Annetta et al., 2019). The FES system section provides further background detail on the FES interface. Additional details for the skin stimulation interface and experiments: each hydrogel disk electrode (Axelgaard; Fallbrook, CA) is 12 mm in diameter, 1.27 mm thick, spaced by ~2-3 mm, and attached to a metal electrode consisting of copper with an electroless nickel immersion gold coating embedded in the polyimide flex circuit. We used two current levels of stimulation: minimum intensity = 2.4 mA, and maximum intensity = 9.6 mA (current controlled stimulation, monophasic rectangular pulses, 50 Hz, 500 μs pulse width, 100 ms train duration). Stimulation intensity was selected based on our pilot studies to apply stimulation sufficient to evoke activity in M1 (minimum intensity) and up to an intensity below a noxious level (maximum intensity). At a given skin stimulation location, fifty replicates of stimulation were performed within a given recording with an inter-stimulus interval of 2 s. This inter-stimulus interval specifically allowed for the evoked neural activity to return to baseline well before the next stimulus, similar to our previous studies (Ganzer et al., 2013; Manohar et al., 2017). On a given recording day, 2 skin locations were selected randomly for stimulation and simultaneous neural recordings. The order of stimulation amplitude for a given skin stimulation location was also selected randomly (e.g., a recording at maximum intensity followed by a recording at minimum intensity, or vice versa). Following a given recording, the participant was asked if he felt the stimuli and whether it was higher or lower in intensity than the previous recording, if applicable (related to Figure 3). We performed a total of 5 recordings at a given skin stimulation site and stimulation intensity. Recordings were performed across a total of ~5 months to assess the chronic viability of the evoked neural signal.

### *Evoked Peri-Stimulus Time Histograms*

All neural recordings were analyzed offline using MATLAB 2016b (The MathWorks). Following stimulation artifact removal (see *Common Methods* above), the signal was band-passed filtered (3$^{rd}$ order Butterworth filter; 300 – 3000 Hz). Multi-unit activity was classified offline using superparamagnetic clustering (Wave clus, Quiroga et al., 2004). Unit clusters were manually inspected (Figures S1D and S1E), similar to our previous studies (Ganzer et al., 2013; Manohar et al., 2017). This was done to affirm waveform quality and morphology. For each channel, the multi-unit neural activity was first binned (20 ms bin width). We calculated evoked responses on a channel by channel basis (total of 96 recording array channels). A peri-stimulus time histogram (PSTH) was constructed for a given channel using the binned neural data 1 s before and after the start of stimulation, averaged across all stimulation trials (example single channel PSTH: Figure S1F). The magnitude of the evoked response was then quantified similar to our previous studies using PSTH-based analyses (Ganzer et al., 2013; Manohar et al., 2017). Details on the PSTH analysis: for a given channel, a response was considered significant if 1) it exceeded an activation threshold set as the average background activity of the channel across all stimulation trials (evaluated from −1 to −0.02 s before the stimulus) plus three standard deviations (Figure S1F, horizontal gray dashed line), and 2) at least three bins were over the activation threshold. The response magnitude for a given channel was then quantified as the background-subtracted number of spikes within the post-stimulus window of the PSTH (0 – 1 s after the stimulus). The response magnitude for a given channel was zero if it did not meet the significance criteria listed above. The global response magnitude was then estimated using the average response magnitude across all array channels for the given condition. We report the global response magnitude (average spikes per channel; Figure 1C; Figure S2B). Global PSTHs are background subtracted and smoothed with a 1$^{st}$ degree polynomial model for plotting purposes (Figure 1B; Figure S2A).

### *Decoding Passive Sensory Stimulation*

A nonlinear support vector machine (SVM) classifier (Friedenberg et al., 2016; Chang and Lin, 2011) was used to decode stimulus location for the passive sensory stimulation recordings at both the minimum and maximum stimulation intensity (referred to as a 'passive sensory decoder' in the results) (SVM hyperparameters: $\gamma$ = 0.001, C = 1). A separate SVM model for each stimulation intensity was built with 5 classes: Rest, Forearm, Thumb, Index, and Middle (related to Figure 2). The input features for each model were calculated as follows: (1) We recorded neural activity and calculated MWP during ~250 total stimuli for each stimulus intensity and skin location across ~5 months; (2) MWP was standardized across blocks within each day to account for day-to-day variability; (3) For each skin stimulation trial, defined by 0.2 s before and 0.8 s after a given sensory stimulus (this epoch was chosen due to the robust neural modulation that occurs during this time period around the stimulus, see Figure 1B, Figure S2A), MWP was vectorized to a 960-feature vector (96 channels * 10 bins; where each bin spanned 100 ms); The same MWP vectorization process was applied to 250 randomly selected 1 s samples of Rest data collected during spontaneous activity in the first 15 s of a given recording; and (4) For each class, the vectorized MWP was shuffled to remove any effect of stimulus order or recording time during the ~5-month period and equally assigned to either training or testing data (~125 trials per class for training; ~125 trials per class for testing). We report SVM model performance as a confusion matrix (diagonal values = sensitivity; off-diagonal values = false positive rate). Sensitivity is calculated as the percentage of correctly predicted class labels for the targeted class (i.e., true positive rate). False positive rate is calculated as the percentage of incorrectly predicted class labels for a given off-target class. Rows represent the actual recorded class, while the columns represent the model's predictions (related to Figure 2).

### Active Object Touch Experiments

*Clinical Assessment of Sensory Function.* Monofilament testing was performed by a licensed physiatrist to evaluate the participant's hand sensory function (GRASSP assessment, Semmes-Weinstein monofilaments; Toronto, ON; Kalsi-Ryan et al., 2012). All sensory function testing was performed in the absence of visual feedback, as per the International Standards for Neurological Classification of Spinal Cord Injury published by the American Spinal Injury Association (Kirshblum et al., 2011). The palmar and dorsal aspects of digits 1 (thumb), 3 (middle), and 5 (pinky) were exposed to multiple trials of either 0.4, 2, 4, or 300 g of force while the participant was blind-folded (related to Figure S1A). Trial location and force level were randomized. The participant was asked to report the application of the applied tactile stimulus. The following scores were generated to quantify the participant's tactile acuity (Kalsi-Ryan et al., 2012): 4 = 0.4 g detection at 66 %; 3 = 2 g at 33 %; 2 = 4 g at 33 %; 1 = 300 g at 33 %; 0 = 300 g at 0 %.

The participant uses his hand to manipulate objects during BCI operation. We assessed the participant's ability to detect object touch during FES-mediated grip (standardized objects tested from the Action Research Arm Test: small cylinder (1 cm diameter) and large cylinder (2 cm diameter); Yozbatiran et al., 2008). The participant was again blind-folded, and the object was placed between digits 1, 2, and 3 without touching the skin on randomized trials where a grip was triggered (small cylinder: lateral pinch grip; large cylinder: *can* grip). A grip was activated for a duration of 3 s for a given trial. The participant then reported whether there was an object in his hand. Each grip trial was bounded by rest periods with random durations between 5 to 6 s. We report Object Touch Detection as the percentage of trials the participant correctly identified there was an object present during grip (related to Figure S1B).

### Decoding Active Touch Alone

We trained SVM decoders to recognize active object touch events in real-time (referred to as a 'touch decoder' in the results) (specifically related to Figures 4 and 5). These decoders were trained using neural data recorded during active object touch, in contrast to the passive sensory decoders described above (see *Decoding Passive Sensory Stimulation*). We used the *can* object, a part of the standard clinical grasp and release test battery (5.4 × 9.1 cm) (Wuolle et al., 1994; Schwemmer et al., 2018; Colachis et al., 2018). For model training, we recorded 9 total cues of labeled touch data, with each cue consisting of a 6 s period. Cues were conveyed by a virtual hand on a computer monitor. Each cued period of touch data was bounded by rest cues with random durations between 5 to 6 s. For each touch cue period, the participant first moved his hand down onto and around the *can* object for 3 s, followed by a scripted object grip period for an additional 3 s, where FES triggered a more forceful grip. Therefore, touch decoder model training consisted of neural data during: 1) movement onto the object, 2) touch of the object, and finally 3) additional FES mediated touch. This touch decoder model was then tested on 4 cue types and rest periods to assess model performance during 'touch' and 'no touch' events. The participant separately completed the following cued events: (1) 3 s of natural touch of the object followed by 3 s FES mediated touch ('Touch'), (2) 6 s of natural object touch ('Touch'), (3) 6 s of identical movement without the object present ('No Touch'), (4) 6 s of FES without the object present ('No Touch'). Rest periods were also assessed, and consisted of 5 s Rest epochs randomly selected across all recordings. For this touch decoder testing, we report model responsiveness during the 4 cue types and rest, defined as the percentage of time the touch decoder output was above the activation threshold during the given period (activation threshold = 0.5; see Video S1 for exemplary touch decoder outputs during testing). This touch decoder was then used to trigger the closed-loop sensory feedback interface during the object manipulation experiments described below (see Function During Sensorimotor Demultiplexing section). In a subset of experiments, we also assessed touch decoder timing during simultaneous recording of applied force (related to Figure S4; force transducer interface: custom designed piezoresistive sensor pad (FlexiForce; Boston, MA) interfaced with an Arduino Mega 2560 board transferring force data to the PC).

### Decoding Active Touch and Grip Intensity

Grip force was measured in a subset of experiments (related to Figures 6B and 6C) using an array of twenty-two piezoresistive sensors (FlexiForce; Boston, MA) built into a 3D printed replicate of the *can* object, described above (5.4 × 9.1 cm; cartoon of the *can* object is shown in Figure 4B and Figure 5A) (Wuolle et al., 1994; Schwemmer et al., 2018; Colachis et al., 2018). This grip force measurement object was similar to grip force transducers from previous studies using force sensors built into customized objects (Kao et al., 2014; Kalra et al., 2015; Pehlivan et al., 2014). The force sensors were evenly distributed around the cylindrical surface of the *can* where the participant grasped the object. Force sensors were interfaced with a Teensey 3.6 USB board (PJRC.com, LLC; Sherwood, OR) for transferring data to the PC (10 Hz sampling frequency). Force measurements from each sensor were calibrated (3-point force calibration; Chatillion TCD225 Series Force Measurement System; Indianapolis, IN). We report total force applied across the total *can* surface during grip events (Figures 6B and 6C).

Different levels of touch and grip intensity were decoded from M1 activity (related to Figures 6A–6C). Similar to our earlier experiments (Figures 4 and 5), the SVM model was first trained and tested with controls (Figure 6A), and then used online during BCI control (Figures 6B and 6C). We trained SVM decoders to recognize different afferent touch and grip intensity levels across three classes: 'Touch Alone', 'Touch & Low Grip', and 'Touch & High Grip'. We used the 3D printed replicate of the *can* object with embedded force sensors to measure grip force during trials. Training data was collected as follows: 1) 'Touch & High Grip' and 'Touch & Low Grip' cues consisted of the participant touching the can and passively experiencing FES for 5 s, at FES intensities of 12.6 mA and 9 mA, respectively; 2) 'Touch & High Grip' and 'Touch & Low Grip' cues were randomly shuffled and separated by periods of 'Touch Alone' that lasted 6-7 s; 3) To mimic long duration grip events, the participant's hand remained in contact with the grip force sensing *can* during all training cues; 4) Only offline analyses included training with an additional control cue type (i.e., a 4$^{th}$ class), 'FES Alone', that lacked object touch. 'FES Alone' cues spanned the FES intensities experienced above (# 1), but no object touch was present (similar to 'FES Alone' with no object touch in Figure 4A). 'FES Alone' cues lasted 5 s to mimic the FES durations from # 1. We report model

performance as a confusion matrix (diagonal values = sensitivity; off-diagonal values = false positive rate). Sensitivity is again calculated as the percentage of correctly predicted class labels for the targeted class (i.e., true positive rate). False positive rate is calculated as the percentage of incorrectly predicted class labels for a given off-target class. Rows represent the actual recorded class, while the columns represent the model's predictions (related to Figure 6A).

We recorded 12 'Touch & High Grip', 12 'Touch & Low Grip', 24 'Touch Alone', and 12 'FES Alone' cues. Decoder performance was appraised (Figure 6A) using a 50 / 50 train-test split across classes using SVM class weights to compensate for minor class imbalances (standardized across train and test data; three of the 96 recording channels were also removed due to a temporary hardware malfunction for data shown in Figure 6A). The online touch and grip intensity decoder was then trained from the same dataset using a 75 / 25 train-test split to increase decoding robustness during online performance (Figures 6B and 6C). This decoder was used to control FES and autonomously adjust grip force during online experiments described below (see Touch Regulated Grip Intensity section).

### Decoding Motor Intention

Similar to our previous studies, we built motor decoders for manipulating the *can* object (a part of the grasp and release test; Wuolle et al., 1994; Schwemmer et al., 2018; Colachis et al., 2018). Details on motor intention decoding: the participant was prompted to imagine performing a *can* grip and movement, using a virtual hand displayed on a computer monitor. Each motor cue lasted 3-4 s, and was bounded by rest cues with random durations between 5 and 6 s. During the initial motor cues, FES triggered the *can* grip. FES was controlled by the SVM motor decoder starting on the $4^{th}$ motor cue. This motor decoder model was updated during subsequent training cues until a sufficiently accurate model was built (accuracy > ~80%). This motor decoder was then used to control FES during the object manipulation experiments described below (see Function During Sensorimotor Demultiplexing sections).

### Sensory Feedback Interface

The sensory feedback interface consisted of 3 low-noise vibrotactile coin motors affixed to a velcro band wrapped around the participant's right bicep (cartoon schematic in Figures 4B and 5A) (coin motor details: 12 mm diameter, 3.4 mm height, 2.6 G force output; Need for Power; Shenzhen, Guangdong, China). This interface was tethered to an Arduino Mega 2560 board to power and control vibrotactile sensory feedback (all 3 vibrotactile motors were either off, or turned on by the touch decoder at their max level: 2.6 G force). Sensory feedback interfaces targeting the skin over the biceps have been used in several sensory feedback studies and is well studied (Meek et al., 1989; Patterson & Katz, 1992; Pylatiuk et al., 2006; Chatterjee et al., 2007). Our pilot data confirm that the participant's right bicep exhibited normal sensory function, and vibrotactile stimulation was recognized on 100% of stimuli. The interface was designed to ensure participant comfort during movement. The vibrotactile motors achieved maximum amplitude within 1 ms of controller signal initiation. All sensory feedback interface communication was also recorded. This sensory feedback interface was controlled by the touch decoders outlined above and was triggered in real time during the closed-loop sensory feedback tasks described below.

### Function During Sensorimotor Demultiplexing

We assessed upper limb function across a battery of 4 clinical assessments under the supervision of a licensed physiatrist (relevant for Figures 4 and 5). The sensory feedback interface was placed on the participant's right bicep during all assessments, and function was assessed across trials during either a 'Control' or 'Demultiplexing With Sensory Feedback' condition. The 'Control' condition consisted of functional testing without any vibrotactile sensory feedback. 'Demultiplexing With Sensory Feedback' consisted of on-demand touch decoder controlled sensory feedback for rapidly conveying hand touch events back to the user. The participant was blinded to the given condition before a series of assessment trials. All clinical assessments were performed across 2 clinical testing days. The trial counts and statistical tests are described in the QUANTIFICATION AND STATISTICAL ANALYSIS section.

The first clinical assessment was an extension of the monofilament testing described above (see Clinical Assessment of Sensory Function section; Kalsi-Ryan et al., 2012). A touch decoder was first constructed identical to that described above (see Decoding Active Touch Alone section). The palmar aspects of digits 1, 3, & 5 were next exposed to multiple trials of either 0.4, 2, 4, or 300 g of force using the monofilaments, in the absence of visual feedback (Kirshblum et al., 2011). Trial location and monofilament force level were randomized. This allowed us to map what hand dermatomes contributed to the activation of the touch decoder (digit 1 (thumb): C6; digit 3 (middle): C7 / C8; digit 5 (pinky): C8; Kalsi-Ryan et al., 2012; Lee et al., 2008). We assessed whether the touch decoder was activated following the application of a given stimulus using simultaneously recorded high-speed video. We report the lowest dermatome level the touch decoder was activated by during the monofilament assessment (e.g., palmar tactile stimulation to digits 3 & 5 repeatedly activated the touch decoder (dermatomes innervated by spinal level C7 / C8)).

The second clinical assessment was an extension of the Object Touch Detection test described above (see Clinical Assessment of Sensory Function section). The standardized large cylinder object was used (Yozbatiran et al., 2008). A touch decoder was first constructed identical to that described above (see Decoding Active Touch Alone & Decoding Motor Intention section). The participant was again blind-folded, and the object was placed between digits 1, 2, and 3 without touching the skin on randomized trials. Grip was triggered by FES during a shuffled series of 'Demultiplexing With Sensory Feedback' or 'Control' condition cues. Grip was activated for a duration of 3 s for a given trial. The participant then reported whether there was an object in his hand. Each grip trial was bounded by rest periods with random durations between 5 to 6 s. We again report Object Touch Detection as the percentage of trials the participant correctly identified there was an object present during grip (related to Figure 4C).

The third clinical assessment consisted of the modified grasp and release test (GRT) only using the *can* object. A touch decoder and motor decoder were constructed identical to that described above (see Decoding Active Touch Alone & Decoding Motor

Intention section). The participant was then cued to repeatedly grasp, move, and release the object during shuffled series of 'Demultiplexing With Sensory Feedback' or 'Control' condition trials. After each GRT trial, the participant reported his sense of agency (SoA) (i.e., "How in control did you feel of the movement and grip"?). The SoA score ranged from 0-100, similar to previous studies (Obhi & Hall, 2011; Kumar et al., 2014) (0 = poor sense of control; 100 = perfect sense of control; related to Figure 5C).

The fourth clinical assessment was a modified GRT again using only the *can* object (related to Figure 5D). A touch decoder and motor decoder were constructed identical to that described above (see Decoding Active Touch Alone & Decoding Motor Intention section). The participant was instructed to repeatedly grasp, transfer, and release the *can* object onto an elevated platform as fast as possible during shuffled series of 'Demultiplexing With Sensory Feedback' or 'Control' condition trials. Each GRT assessment period consisted of two 60 s object transfer periods separated by a 20 s rest period. All GRT trials were recorded with high speed video for offline analysis. We quantified the number of objects successfully transferred and the object transfer times, similar to our previous studies (Schwemmer et al., 2018; Colachis et al., 2018). A successful transfer started the moment the object was initially contacted by the hand and ended when the object was fully released onto the platform (no objects were dropped). We also assessed the interval between the touch decoder and motor decoder activations to examine the neurophysiological substrates of GRT performance with and without sensory feedback (high-speed video was also used in addition to decoder times to confirm touch and motor event start times). The touch decoder or motor decoder start times were calculated across GRT trials using the time each decoder crossed the device activation threshold (device activation threshold = 0.5). We report the interval (s) between the touch and motor decoder activations across testing conditions.

#### *Touch Regulated Grip Intensity*

The participant also utilized touch and grip intensity decoding online for grip adjustment experiments (related to Figures 6B and 6C; all data for Figure 6 was recorded during the same clinical session). The participant briefly initiated a given trial using motor intention to start FES and grasp the *can* object with built in grip force sensors. After that point, FES mediated grip was controlled solely by touch and grip intensity decoders. The participant was free to attend to other stimuli while the touch and grip intensity decoder modulated FES levels. There were two trial types: 1) 'Touch & High Grip' trials were initiated at 12.6 mA FES (identical to 'Touch & High Grip' cues during SVM training); 2) 'Touch & Low Grip' trials were initiated at 9 mA FES (identical to 'Touch & Low Grip' cues during SVM training). A prediction of 'Touch & High Grip' decreased FES and subsequent grip force, and a prediction of 'Touch & Low Grip' increased FES and subsequent grip force. The given FES change occurred at a rate of 0.1 mA per prediction bin (every 100 ms). The touch and grip intensity decoder was challenged to appropriately decrease ('Touch & High Grip' trials) or increase ('Touch & Low Grip' trials) FES and subsequent grip force solely based on decoded afferent touch and grip intensity activity from M1 in real-time (grip force data is reported during the initial adjustment and equilibration period; i.e., 1-7 s after trial initiation). We report average FES amplitude change and the grip force values across time (1 s averages; 3$^{rd}$ degree polynomial fit included for Figures 6B and 6C to show trends).

## QUANTIFICATION AND STATISTICAL ANALYSIS

Normality tests were performed for each analysis to determine if parametric or nonparametric statistics should be used. All statistical tests were two-tailed unless otherwise noted and performed in MATLAB 2016b. An alpha level of 0.05 was accepted for significance unless Bonferroni corrections are noted. Trial counts are noted below or in the METHOD DETAILS section. Details of statistical scores and parameters are provided in the given Results section.

Effects of sensory stimuli on evoked M1 neural activity across skin locations were evaluated using separate one-way ANOVAs for the maximum (Figure 1C) and minimum (Figure S2B) stimulation intensities. The factor was skin location with 4 levels: forearm, thumb, index, and middle. Tukey's post hoc test was used to determine differences in global response magnitude across skin locations. Independent samples t tests were used to determine the effects of sensory stimuli on evoked M1 neural activity for data recorded during stimulation of the contralateral and ipsilateral forearm and thumb (related to Figure S3).

Separate one-tailed independent samples t tests were used to determine if decoder performance values were above chance for the passive sensory stimulation data (confusion matrices, Figure 2) or the touch and grip intensity data (confusion matrix, Figure 6A). Each given confusion matrix value was compared to a chance prediction level for statistical evaluation. Chance levels were generated by randomly permuting the data labels 10 times (Ojala & Garriga, 2010). Values from unrandomized label permutation were then compared with values from randomized label permutation. A Bonferroni corrected alpha value was used for significance (0.05 / number of comparisons). Differences in perceptual and decoder sensitivities were assessed using separate one-way ANOVAs for each of the 4 skin locations (related to Figure 3).

For the active object touch experiments, touch decoder responsiveness values were assessed using a one-way ANOVA (related to Figure 4). The factor was cue type with 4 levels: Object Touch & FES, Object Touch, FES alone, and Movement alone. Tukey's post hoc test was used to determine differences in touch decoder responsiveness across cue type. Functional improvement assessments (related to Figure 5) were performed across 2 separate clinical testing days for the following total trial counts: object touch detection, 16 trials (for either the 'Demultiplexing With Sensory Feedback' and 'Control' conditions); SoA, 24 trials (for either 'Demultiplexing With Sensory Feedback' and 'Control' conditions); modified GRT performance & decoder interval, 78 trials ('Demultiplexing With Sensory Feedback') and 72 trials ('Control'). Effects of closed-loop sensory feedback were assessed using independent samples t tests for the object touch detection, SoA, GRT performance, and decoder interval data, comparing the 'Demultiplexing With Sensory Feedback' to 'Control' conditions.

Touch regulated grip intensity data was assessed using a slope test statistic (related to Figures 6B and 6C). Touch regulated grip intensity was performed during 1 clinical testing day for the following trial counts: 'Touch & High Grip': 11 trials, 'Touch & Low Grip' trials: 14 trials.

## ADDITIONAL RESOURCES

Clinical trial link (ClinicalTrials.gov Identifier: NCT01997125): https://clinicaltrials.gov/ct2/show/NCT01997125

Cell

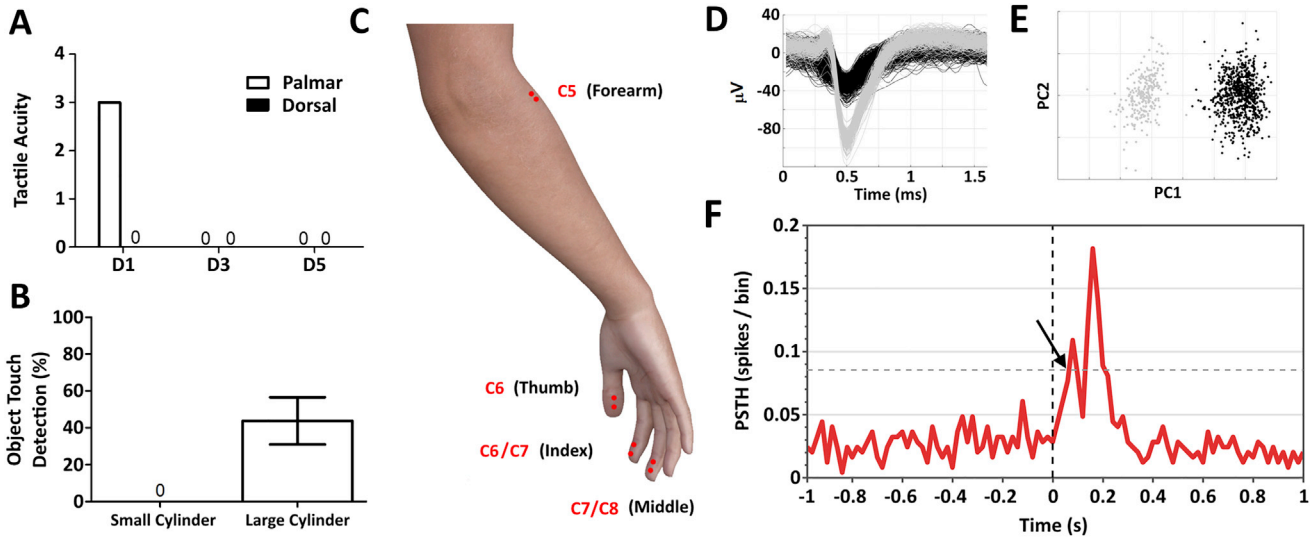


**Figure S1. Hand Sensory Function Assessment and Neural Recording Methods, Related to Figure 1 and STAR Methods**

(A) The participant's hand sensory function was significantly impaired following injury (quantified using standard monofilament testing; clinical scores are integers, see STAR Methods and Kalsi-Ryan et al., 2012 for details).

(B) During FES mediated grip, the participant was largely unable to discriminate object touch events in the absence of visual feedback, operating at subperceptual levels for both standardized objects. These results demonstrate that hand sensory function is dramatically impaired following SCI. Data presented are mean ± SEM.

(C–E) (C) Electrotactile stimulation was performed at 4 different skin locations on the right arm or hand across a period of ~5 months to assess sensory evoked responses in M1. Neural activity was recorded from a Utah microelectrode recording array implanted in left M1 (Figure 1A) during skin stimulation protocols (D) = exemplar unit waveforms; (E) = corresponding principal component analysis of the unit waveforms).

(F) For each array channel, we constructed a peri-stimulus time histogram (PSTH) of the multiunit activity to assess neural modulation evoked by skin stimulation. Exemplar single channel PSTH is plotted 1 s before and 1 s after the start of skin stimulation (stimulation occurs at time 0, vertical black dashed line). To quantify the neural response, an activation threshold was first calculated based on the background neural activity (activation threshold = horizontal gray dashed line). At least 3 total bins crossed the activation threshold to be considered an evoked response (black arrow: first significant crossing), similar to our previous studies (Ganzer et al., 2013; Manohar et al., 2017). See *Evoked Peri-Stimulus Time Histograms* of the STAR Methods for additional data processing details.

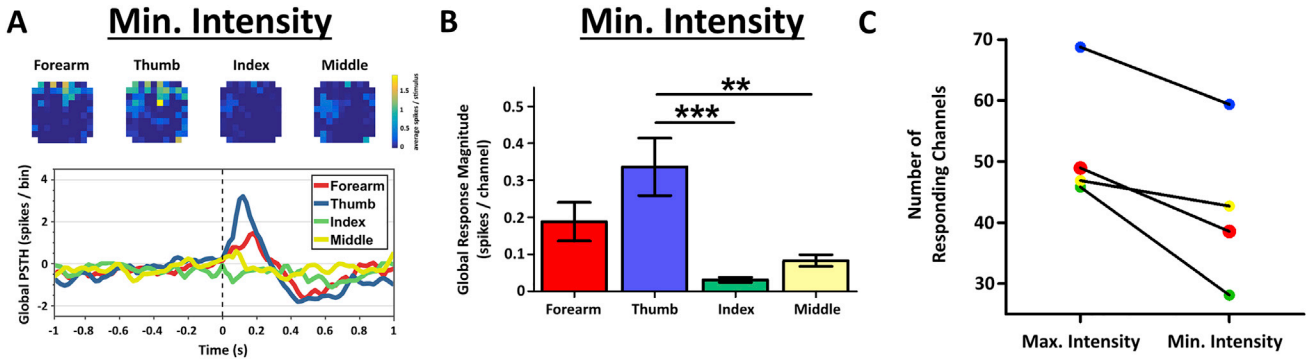


**Figure S2. Evoked Multiunit Responses across Stimulation Intensities, Related to Figure 1**

(A) Color coded representations of multiunit response magnitudes across the microelectrode recording array (color scaling: blues = no or small M1 responses; yellow = large M1 responses; units: average spikes / stimulus), and accompanying peri-stimulus time histogram (PSTH) during stimulation to the forearm (red), thumb (blue), index finger (green), or middle finger (yellow) at the minimum stimulation intensity.

(B) At the minimum stimulation intensity, stimulation of the thumb evoked a significantly larger global response magnitude compared to index or middle ($F[3, 380] = 7.9$, $p < 0.001$; *** = $p < 0.001$, ** = $p < 0.01$).

(C) Number of channels responding to the maximum and minimum intensities across skin locations. Data presented are mean ± SEM.

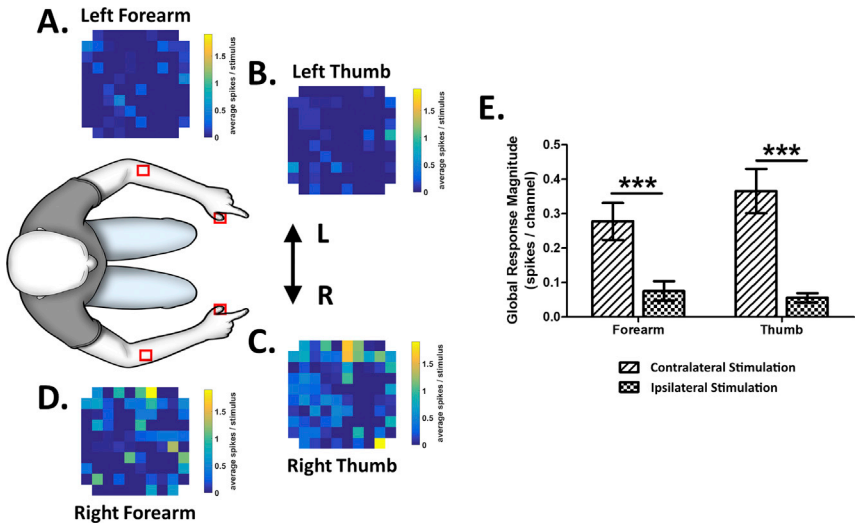


**Figure S3. Control Sensory Stimuli Ipsilateral to the Microelectrode Recording Array in Left M1 Evoke Little to No Neural Activity, Related to Figure 1**

(A–D) We performed control recordings using electrotactile stimuli to the homotopic forearm (A) and thumb (B) locations on the arm ipsilateral to the M1 recording array at the maximum stimulation intensity (color coded representations of multi-unit response magnitudes are shown across the microelectrode recording array; color scaling: blues = no or small M1 responses; yellow = large M1 responses; units: average spikes / stimulus). As expected, stimuli to these skin sites demonstrate little to no evoked neural activity in left M1. Global response magnitudes following contralateral skin stimulation (at the contralateral thumb (C) and forearm (D), repeated from Figures 1C and 1D) were on average over 5 times larger compared to responses following homotopic ipsilateral skin stimulation (E, forearm: $t(95) = 3.9$, thumb: $t(95) = 4.9$; *** = $p < 0.001$). These results support the hypothesis that evoked activity in M1 following sensory stimuli is maximal from semi-intact skin locations contralateral to the microelectrode recording array. Stimulated skin locations outlined in red boxes. Data presented are mean ± SEM.

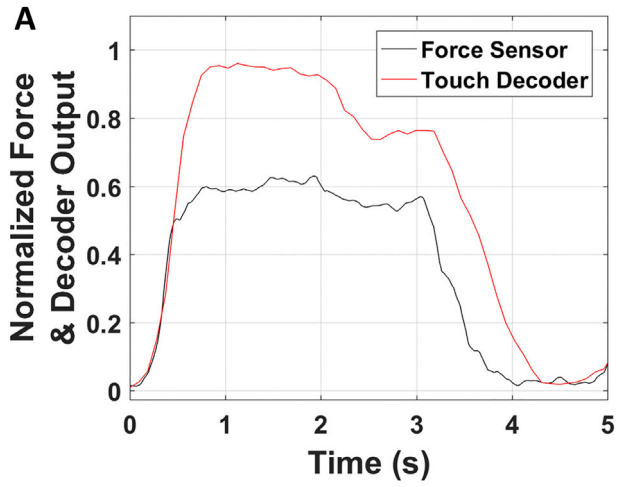


**Figure S4. Touch Decoders during Object Grip Are Time Locked to Force Application, Related to Figure 4**

In a subset of experiments, we assessed touch decoder outputs and subsequent force generation during object grip. We applied preprogrammed FES to generate a lateral pinch grip, subsequently creating force transduced by a piezoresistive sensor interface. Neural activity, touch decoders, and force sensor readings were all recorded simultaneously.

(A) The average latency between touch decoder activation and force application was 22 ms. Touch decoder activation was therefore time-locked to force generation, with synchronized on and off times.

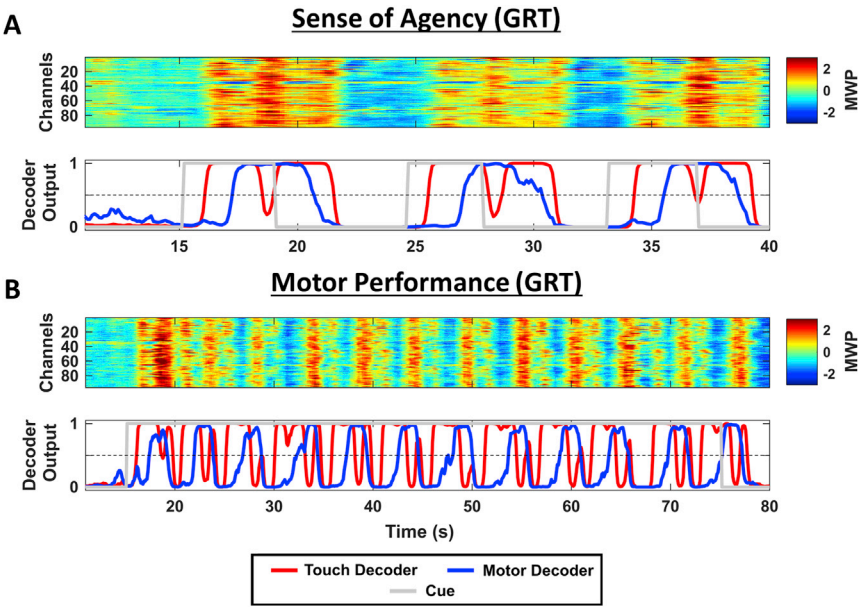


**Figure S5. Mean Wavelet Power Input and Decoder Output Plots for the Sensorimotor Demultiplexing BCI Tasks, Related to Figure 5**

Exemplary MWP input and SVM decoder outputs during the sense of agency (A; main data: Figure 5C), and GRT motor performance assessments (B; main data: Figure 5D). Color coded MWP data recorded across the 96-channel microelectrode recording array is shown at the top of each panel and serve as an input to the SVM. Simultaneous SVM decoder outputs are shown below each MWP plot. Touch decoder outputs (red lines) control the sensory feedback device. Motor decoder outputs (blue lines) control FES of the arm. The device activation threshold is shown as a horizontal dashed line on all decoder output plots (at 0.5). Assessments are cued (overlaid cue periods in gray). Please see the Active Object Manipulation Experiments of the STAR Methods for further details.